Plant Physiology®

Clathrin-mediated trafficking regulates copper tolerance by modulating the localization of HEAVY METAL ATPase 5 in Arabidopsis root cells

Liufan Wang,[1,†] Mei Xu,[1,†] Yonghua Shao,[1] Guochao Zhang,[1] Yuling Ran,[1] Hongqian Lu,[1] Jiaqi Ma,[2] Jieming Jiang,[3]

Xifeng Chen,[4] Xu Yan,[1,*] Jianxin Shou,[1,*] Chao Wang[1,*]

[1]School of Life and Environmental Sciences, Shaoxing University, Shaoxing 312000, China
[2]School of Life Sciences, Lanzhou University, Lanzhou 730000, China
[3]School of Life Science, South China Normal University, Guangzhou 510631, China
[4]College of Life Sciences, Zhejiang Normal University, Jinhua 321004, China
*Author for correspondence: yanxu@usx.edu.cn (X.Y.), jianxinshou@usx.edu.cn (J.S.), wangc@usx.edu.cn (C.W.)
[†]These authors contributed equally to this work.
The author responsible for distribution of materials integral to the findings presented in this article in accordance with the policy described in the Instructions for Authors (https://academic.oup.com/plphys/pages/General-Instructions) is Chao Wang (wangc@usx.edu.cn).

ABSTRACT

Plant clathrin and its adaptor protein complexes—adaptor protein complex-1 (AP-1) at the *trans*-Golgi network/early endosome (TGN/EE) and the adaptor protein complex-2 (AP-2) at the plasma membrane (PM)—function in clathrin-mediated trafficking (CMT). This study reports the role of CMT in regulating copper (Cu) tolerance in plants. We found that high concentrations of exogenous Cu treatment increase the abundance of clathrin and adaptor protein complexes at the TGN/EE and/or the PM. We further found that a CMT-deficient mutant *ap2μ2, clc2 clc3* exhibits hypersensitivity to Cu stress, similar to a mutant lacking the Cu transporter HEAVY METAL ATPase 5 (HMA5). As previously reported, HMA5 relocates from the endoplasmic reticulum (ER) to the PM on the soil side, where it excretes excess Cu from the root cell, which is crucial for Cu tolerance. Our protein interaction assays showed that the AP-1 and AP-2 σ subunits depend on the YXXΦ sorting motif of HMA5 for recognition. Defective AP-1 hinders HMA5 translocation to the PM after its transfer from the ER to the TGN/EE following Cu stress, while impaired AP-2 function inhibits HMA5 endocytosis at the PM. These results demonstrate that CMT mediates the endocytic recycling of HMA5 between the TGN/EE and the PM, thereby regulating Cu efflux from root cells. Our findings highlight a function of CMT in maintaining Cu homeostasis.

Introduction

Copper (Cu) is an essential nutrient for plant growth and development and plays a critical role in various physiological activities, such as photosynthesis, respiration, and antiviral defenses (Festa and Thiele 2011; Yao et al. 2022). To ensure that Cu can effectively perform its biological functions, plants must tightly regulate Cu uptake and efflux such that the Cu content in the cells is maintained at an appropriate level (Chen et al. 2022). In flowering plants, the maintenance of Cu homeostasis is dependent on the synergistic cooperation of Cu transporter proteins (Burkhead et al. 2009; Xu et al. 2024). In *Arabidopsis thaliana* roots, copper transporter 1 (COPT1), a member of the COPPER TRANSPORTER (COPT) family, mediates Cu uptake, while the P_{1B} ATPase family member heavy metal-transporting P-type ATPase 5 (HMA5) regulates the efflux of excess Cu (Sancenón et al. 2003; Andrés-Colás et al. 2006, 2010; Kobayashi et al. 2008).

An excess of intracellular Cu can produce a large number of free radicals and reactive oxygen species, causing serious toxicity to the plant, with symptoms including the inhibition of seed germination, decreased efficiency of mineral nutrient uptake, reduced photosynthesis, and root growth retardation (Chen et al.

2022). With recent industrial development, the area of Cu-contaminated soil has increased globally, leading to a gradual rise in the frequency of excess Cu toxicity in plants (Rehman et al. 2019; Shabbir et al. 2020). Among a host of Cu transporter proteins, HMA5 was identified to have a unique Cu detoxification function (Andrés-Colás et al. 2006; Kobayashi et al. 2008; Li et al. 2017). There is evidence that *HMA5* expression is induced when plants are stimulated by high concentrations of external Cu (Andrés-Colás et al. 2006). Moreover, the HMA5 protein polarly translocates from the endoplasmic reticulum (ER) to the plasma membrane (PM) near the soil side in root epidermal cells after Cu treatment, excreting excess Cu from the plant and thus improving Cu tolerance (Li et al. 2017). However, the molecular mechanisms adopted by plants to regulate HMA5 protein relocalization under excess Cu remain unclear.

Vesicular trafficking is a eukaryotic transport mechanism that regulates intracellular material translocation, ensuring the precise and timely modulation of the subcellular localization and abundance of numerous proteins (Stenmark 2009; Yao and Xue 2011). Clathrin, a triskelion-shaped complex consisting of three heavy chains (CHCs) and three light chains (CLCs), is an

evolutionarily conserved vesicle coat protein in eukaryotes (Royle 2006; Kaksonen and Roux 2018). The plant adaptor protein heterotetrameric complex ADAPTOR PROTEIN 2 (AP-2, consisting of AP2α, AP2β, AP2μ, and AP2σ) and the heterooctameric TPLATE complex (TPC) recognize cargo and recruit clathrin to the PM, internalizing PM-resident proteins into the cytosol via clathrin-mediated endocytosis (CME) (Kim et al. 2013; Yamaoka et al. 2013; Gadeyne et al. 2014; Grones et al. 2022). In addition, plant clathrin is recruited by heterotetrameric complex ADAPTOR PROTEIN 1 (AP-1, consisting of AP1α, AP1β, AP1μ, and AP1σ) to the *trans*-Golgi network/early endosome (TGN/EE) to mediate post-Golgi trafficking (Yan et al. 2021; Liu et al. 2022; Xu et al. 2022). In plants, clathrin-mediated trafficking (CMT) regulates the biological functions of the boron transporter proteins BOR1 and NIP5;1 and the iron transporter protein IRT1 by modulating their endocytosis, recycling, and vesicular degradation, thereby controlling the root uptake of these nutrients from the soil in response to environmental changes (Takano et al. 2010; Barberon et al. 2014; Yoshinari et al. 2016; Wang et al. 2017; Yoshinari et al. 2019).

In this study, we characterized the previously unexplored roles of CMT in the defense response to Cu stress. We found that, upon Cu stimulation, clathrin in root cells is recruited to the TGN/EE and PM by AP-1 and AP-2, respectively, within a very short period, mediating the translocation of HMA5 from the TGN/EE to the PM, and subsequently regulating the activity of HMA5 through endocytic recycling. This work established a functional link between CMT and Cu homeostasis and revealed the molecular mechanism of HMA5 intracellular transport in plants.

Results

Cu enhances clathrin association with membranes

The formation of root gravitropism and hypocotyl phototropism depends on changes in the abundance of clathrin at the PM and TGN/EE in root epidermal cells and hypocotyl endodermal cells, respectively (Wang et al. 2016a; Zhang et al. 2017). Clathrin recruitment at the membrane is critical for CMT to regulate environmental responses in plants. Studies have shown that CMT is involved in the adaptive response of plants to differences in environmental concentrations of boron and iron (Barberon et al. 2014; Yoshinari et al. 2016; Wang et al. 2017; Yoshinari et al. 2019). However, the specific regulatory mechanisms underlying how CMT-related components and pathways maintain the homeostasis of these nutrients remain unknown.

To explore the response of plant clathrin to different metal cations, we tested the effects of $10\,\mu M$ $CuSO_4$, $MgSO_4$, $ZnSO_4$, and $FeSO_4$ on the levels of membrane-associated CLC1 (clathrin light chain 1)-GFP (green fluorescent protein) in the roots by confocal laser scanning microscopy (CLSM), respectively. Surprisingly, we found that the levels of PM- and TGN/EE-associated CLC1-GFP significantly (Student's *t*-test) increased after 5 min of Cu treatment and remained in high abundance for the following 2 h (Fig. 1, A to F and M). In contrast, magnesium, zinc, and iron treatments did not trigger any changes in CLC1-GFP (Supplementary Fig. S1). We further examined the effect of Cu on the membrane abundance of endogenous CLC1 using affinity-purified anti-CLC1-specific antibodies. Immunofluorescence microscopy showed that Cu treatment induced a significant increase in the PM and TGN/EE abundance of the CLC1 isoform relative to that observed in the mock controls over the same period (Fig. 1, G to L and N), consistent with the live-cell imaging analysis.

To determine the source of the increase in clathrin membrane abundance during Cu stress, we examined the effect of Cu on the expression of *CLC1*, *CLC2*, and *CLC3*. RT-qPCR analysis showed that the mRNA expression levels of *CLC1*, *CLC2*, and *CLC3* in $CuSO_4$-treated Col-0 seedlings were similar to those detected without $CuSO_4$ treatment (Supplementary Fig. S2). Furthermore, immunoblot analysis showed that the level of CLC1-GFP in total protein extracts from wild-type seedlings treated with $CuSO_4$ was similar to those without $CuSO_4$ treatment (Supplementary Fig. S3). These results indicated that the increase in the levels of membrane-associated CLCs was likely due to their membrane recruitment rather than changes in their expression levels. Thus, our results showed that excess Cu induces the rapid recruitment of clathrin to the PM and TGN/EE, suggesting that CMT may play an important role in Cu tolerance.

CMT defects reduce Cu resistance

To verify whether CMT is involved in regulating Cu tolerance, we examined the effect of high Cu concentrations on the growth of the CMT-deficient mutants *ap2μ2*, *clc2 clc3*, and *ap2μ2 clc2 clc3*. Five-day-old Col-0 and CMT-deficient mutant seedlings were separately transferred to solid 1/2 MS medium containing $50\,\mu M$ $CuSO_4$ for 3 d. The results showed that the growth of CMT-deficient mutant roots was hypersensitive to Cu, and their elongation was inhibited more severely than that of Col-0 roots (Fig. 2, A and B). Quantitative analysis showed that the relative elongation of the *ap2μ2*, *clc2 clc3*, and *ap2μ2 clc2 clc3* mutant roots was significantly reduced compared with that of Col-0, with the *ap2μ2 clc2 clc3* triple mutant exhibiting the least elongation (Fig. 2C). This implied that CMT positively regulates Cu tolerance.

Next, we further examined the inhibitory effect of Cu on the growth of the triple mutants using hydroponic experiments. After 15 d of growth in liquid medium containing 2.5 or $5\,\mu M$ $CuSO_4$, relative root elongation in the *ap2μ2 clc2 clc3* mutant was reduced relative to that seen in Col-0 (Fig. 2, D and E). In addition, the inhibition of *ap2μ2 clc2 clc3* mutant root growth by $5\,\mu M$ $CuSO_4$ treatment was stronger than that by $2.5\,\mu M$ (Fig. 2F). These results suggested that CMT defects reduce Cu resistance in plants.

CMT regulates Cu resistance in a HMA5-dependent manner

The results presented in the previous section indicated that clathrin and its adaptor protein are involved in Cu resistance, suggesting that the trafficking of the Cu transporter may be dependent on the CMT pathway. To explore CMT-related Cu transporters, we treated mutants of Cu transporters that function at the PM of root cells—the copper uptake transporters COPT1, COPT2, ZIP2, and ZIP4 and the Cu efflux transporter HMA5 (Milner et al. 2013; Sanz et al. 2019)—with high Cu concentrations. As shown in Supplementary Fig. S4, the root growth of *copt2*, *zip2*, and *zip4* mutants after 3 d of $50\,\mu M$ $CuSO_4$ treatment was similar to that of Col-0; in contrast, *copt1* and *hma5* mutants exhibited insensitivity and hypersensitivity to Cu, respectively.

To elucidate the potential link between HMA5 and CMT, we crossed the *hma5* mutant to the *ap2μ2 clc2 clc3* mutant and analyzed the effect of the loss of HMA5 function on the Cu-sensitive phenotype of the *ap2μ2 clc2 clc3* mutant. We observed that relative root elongation in the *hma5* mutant was reduced compared to that of the *ap2μ2 clc2 clc3* mutant after 3 d of Cu treatment, while the Cu sensitivity of the *hma5 ap2μ2 clc2 clc3* quadruple mutant was similar to that of the *hma5* single mutant (Fig. 3, A to C). Cu levels, as determined using inductively coupled plasma-mass spectrometry (ICP-MS), were elevated in plant roots after $CuSO_4$ treatment and
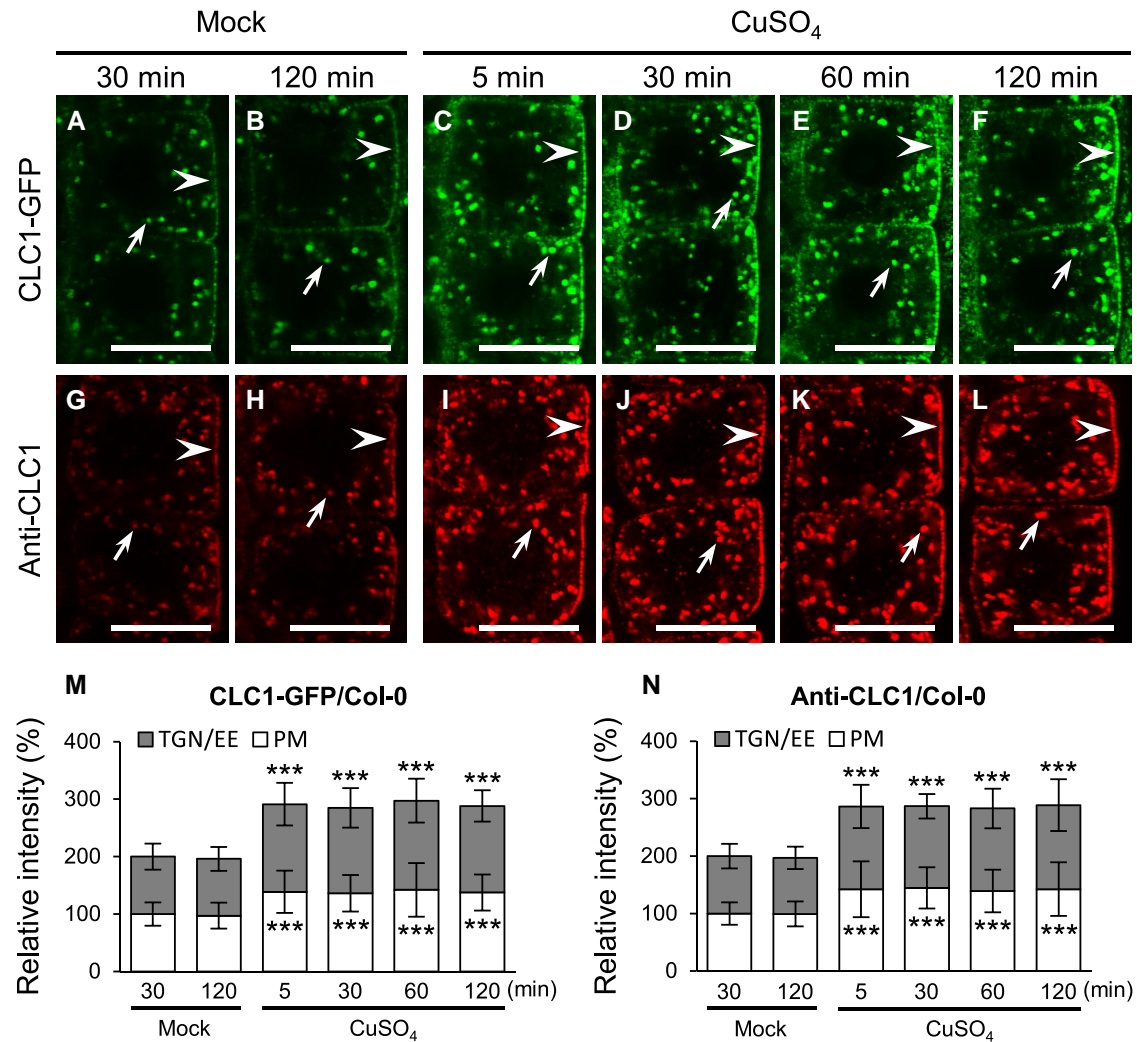
Figure 1. Levels of membrane-associated CLC1 increase rapidly in response to copper stimulation. **A-L)** Copper effect on TGN/EE- and PM-associated CLC1-GFP **(A-F)** and CLC1 **(G-L)** in the wild-type root meristem epidermal cells. **M** and **N)** The relative intensities of TGN/EE- and PM-associated CLC1-GFP **(M)** ($n = 72$ cells from 9 roots) and CLC1 **(N)** ($n = 72$ cells from 9 roots). Different time lengths (5, 30, 60, and 120 min) after the addition of $CuSO_4$ (10 μM) or in the absence of exogenous $CuSO_4$ (mock controls) are indicated at the top of the figure. Arrows and arrowheads show TGN/EE- and PM-associated CLC1-GFP or CLC1, respectively. Shown are means $\pm$ SD. Triple asterisks indicate $P < 0.0001$ (Student's t-test). Bars = 10 μm **(A-L)**.

were significantly higher in the *ap2μ2 clc2 clc3* mutant than in Col-0. Moreover, Cu levels were similar between the *hma5* and *hma5 ap2μ2 clc2 clc3* mutants, with values exceeding those of the *ap2μ2 clc2 clc3* mutant (Fig. 3D). In contrast, the knockout of COPT1 function enhanced Cu tolerance in *ap2μ2 clc2 clc3* mutants (Supplementary Fig. S5, A to C). ICP-MS analysis showed that Cu levels in the roots of the $CuSO_4$-treated *copt1 ap2μ2 clc2 clc3* quadruple mutant were restored to approximately those of the Col-0 and *copt1* mutants (Supplementary Fig. S5D). Furthermore, no significant differences in Cu contents were observed in *hma5*, *copt1*, *ap2μ2 clc2 clc3*, *hma5 ap2μ2 clc2 clc3*, and *copt1 ap2μ2 clc2 clc3* mutant shoots, with or without $CuSO_4$ treatment, compared with those of Col-0 (Supplementary Fig. S6). Taken together, these results suggested that CMT deficiency triggers reduced Cu tolerance in Arabidopsis via the root HMA5-mediated Cu efflux pathway, but not the Cu uptake pathway.

HMA5 transport from the TGN/EE to the PM is disrupted in CMT-deficient mutants

Studies have shown that under Cu stimulation, *HMA5* expression is induced to promote the excretion of intracellular excess Cu ions

from plants (Andrés-Colás et al. 2006). To address whether CMT defects affect the response of HMA5 to Cu at the transcriptional level, we examined the expression of *HMA5* in the *ap2μ2 clc2 clc3* mutant. RT-qPCR analysis showed that the levels of *HMA5* mRNA expression in the *ap2μ2 clc2 clc3* mutant seedlings were similar to those of Col-0 with or without the application of exogenous copper, suggesting that the reduction in Cu resistance was not due to changes in *HMA5* transcript levels in the *ap2μ2 clc2 clc3* mutant (Supplementary Fig. S7).

During Cu stress in plants, HMA5 in root cells relocalizes from the ER to the soil side of the PM, where it acts as a Cu efflux transporter for detoxification (Li et al. 2017). To determine whether CMT defects impact the intracellular transport of HMA5, we used live-cell imaging to analyze the subcellular localization of YFP-HMA5 in Col-0 and the *ap2μ2 clc2 clc3* mutant at different time points after Cu treatment. After 10 min of $CuSO_4$ treatment, YFP-HMA5 in Col-0 and *ap2μ2 clc2 clc3* mutants relocalized from the ER to unknown punctate organelles (Fig. 4, A, B, F, and G). Colocalization analysis showed that the YFP-HMA5-labeled organelles colocalized almost completely with CLC2-mKO and partially with VHAa1-RFP and SNX1-RFP,
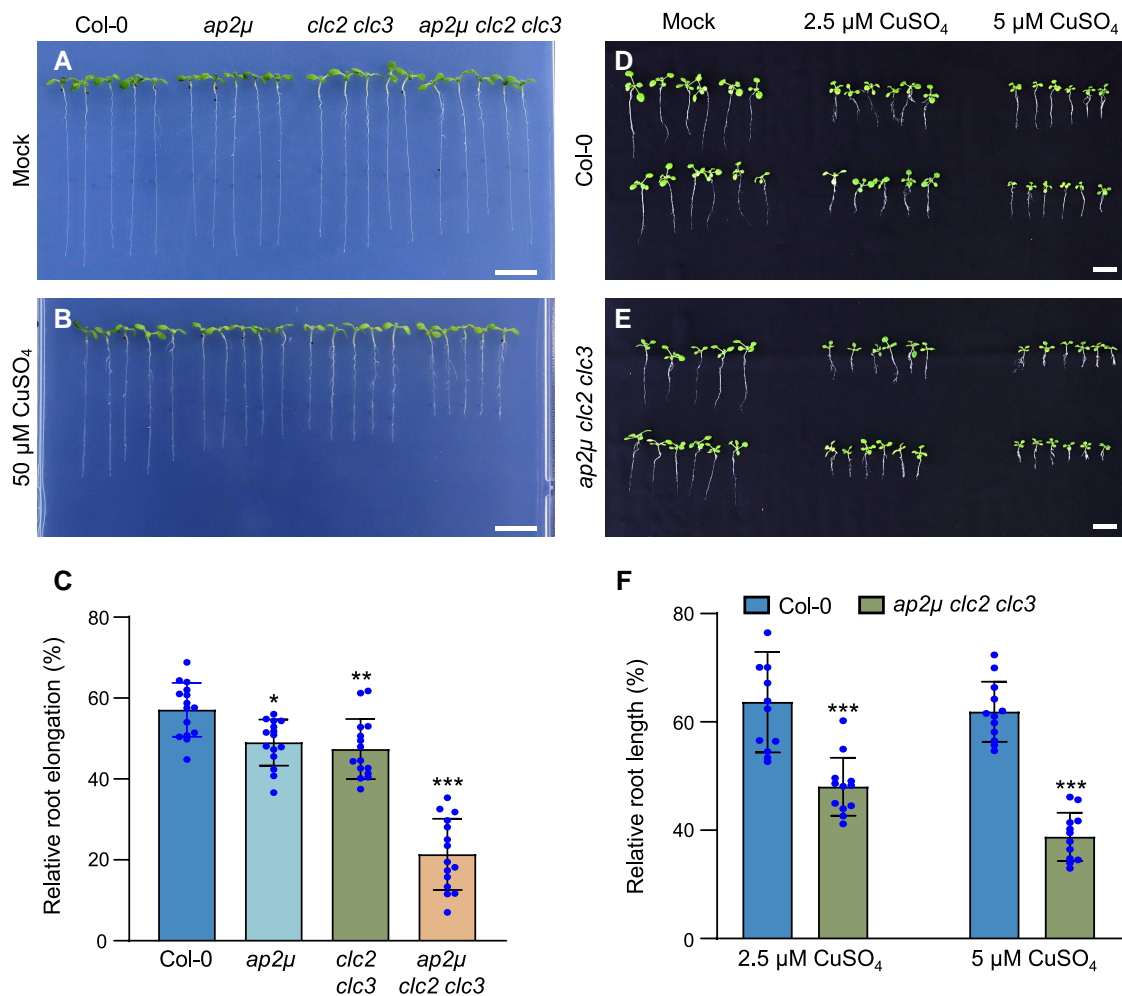
Figure 2. Defects in CMT decreased tolerance to copper. **A** and **B)** Five-day-old vertically grown seedlings in Col-0, *ap2μ*, *clc2 clc3*, and *ap2μ clc2 clc3* mutants were transferred to 0.5× MS solid medium plates containing 0 **(A)** or 50 *μ*M CuSO₄ **(B)** for 3 d. **C)** Relative root elongation under excess Cu compared with the mock controls (*n* = 15 roots from Col-0, 15 roots from *ap2μ*, 15 roots from *clc2 clc3*, and 15 roots from *ap2μ clc2 clc3*). **D** and **E)** Col-0 and *ap2μ2 clc2 clc3* seedlings were grown in normal hydroponic solution **(D)** and hydroponic solution containing 2.5 *μ*M and 5 *μ*M Cu **(E)** for 15 d, respectively. **F)** Relative root length under excess Cu compared with the mock controls (*n* = 12 roots from Col-0 and 12 roots from *ap2μ clc2 clc3* at 2.5 *μ*M Cu; *n* = 12 roots from Col-0 and 12 roots from *ap2μ clc2 clc3* at 5 *μ*M Cu). Shown are means ± SD. Single, double, and triple asterisks indicate $P < 0.05$, 0.01, and 0.0001, respectively (Student's *t*-test). Bars = 1 cm **(A, B, D,** and **E)**.

indicating that the organelles were the TGN/EE (Supplementary Fig. S8). Interestingly, after 20 min of copper treatment, a portion of YFP-HMA5 had translocated to the PM in Col-0, whereas in the *ap2μ2 clc2 clc3* mutant YFP-HMA5 remained in the TGN/EE, and fluorescent signals were not detected at the PM until after 30 min (Fig. 4, C, H, and I). Subsequently, the TGN/EE-associated YFP-HMA5 in the Col-0 and *ap2μ2 clc2 clc3* mutants continued to transfer to the PM with increasing CuSO₄ treatment duration (Fig. 4, D, E, and J). Quantitative fluorescence analysis showed that the rate of YFP-HMA5 relocalization to the PM was significantly reduced in the *ap2μ2 clc2 clc3* mutant relative to that in Col-0 (Fig. 4K).

To further validate that CMT regulates HMA5 translocation from the TGN/EE to the PM, Col-0 seedlings were treated with endosidin9 (ES9), an inhibitor of clathrin heavy chain (CHC) (Dejonghe et al. 2019). CLSM revealed that co-treatment with CuSO₄ and ES9 enabled the transfer of YFP-HMA from the ER to the TGN/EE, but the next step of translocation to the PM (Supplementary Fig. S9). In addition, we detected no difference in the polarity index of YFP-HMA5 at the PM in *ap2μ2 clc2 clc3* mutants compared to that in Col-0 (Fig. 4, L to R). Together, these

results suggested that the translocation of HMA5 from the TGN/EE to the PM during Cu exposure is dependent on CMT.

AP-1 mediates HMA5 sorting at the TGN/EE

To reveal the mechanism underlying the regulation of HMA5 transport by CMT at the TGN/EE, it was essential to first address how clathrin recognizes HMA5 as a cargo protein. We previously demonstrated that the plant AP-1 μ and/or σ subunit recognizes cargo at the TGN/EE by binding to the sorting motif of the protein and subsequently recruits clathrin to the TGN/EE (Yan et al. 2021; Xu et al. 2022). Therefore, we examined whether AP-1 responded to strong Cu stimulation in root cells. CLSM analysis revealed that CuSO₄ treatment for 5 min resulted in a significant increase in the fluorescence signals of the AP-1 complex subunit, AP1μ2, tagged with a red fluorescent protein (AP1μ2-RFP), and the AP1σ2 subunit, tagged with a green fluorescent protein (AP1σ2-GFP) at the TGN/EE, which were then maintained at a high abundance for the following 2 h (Fig. 5, A to N). To confirm the role of the AP-1 complex in HMA5 protein transport, we observed the localization of YFP-HMA5 after Cu stress in the
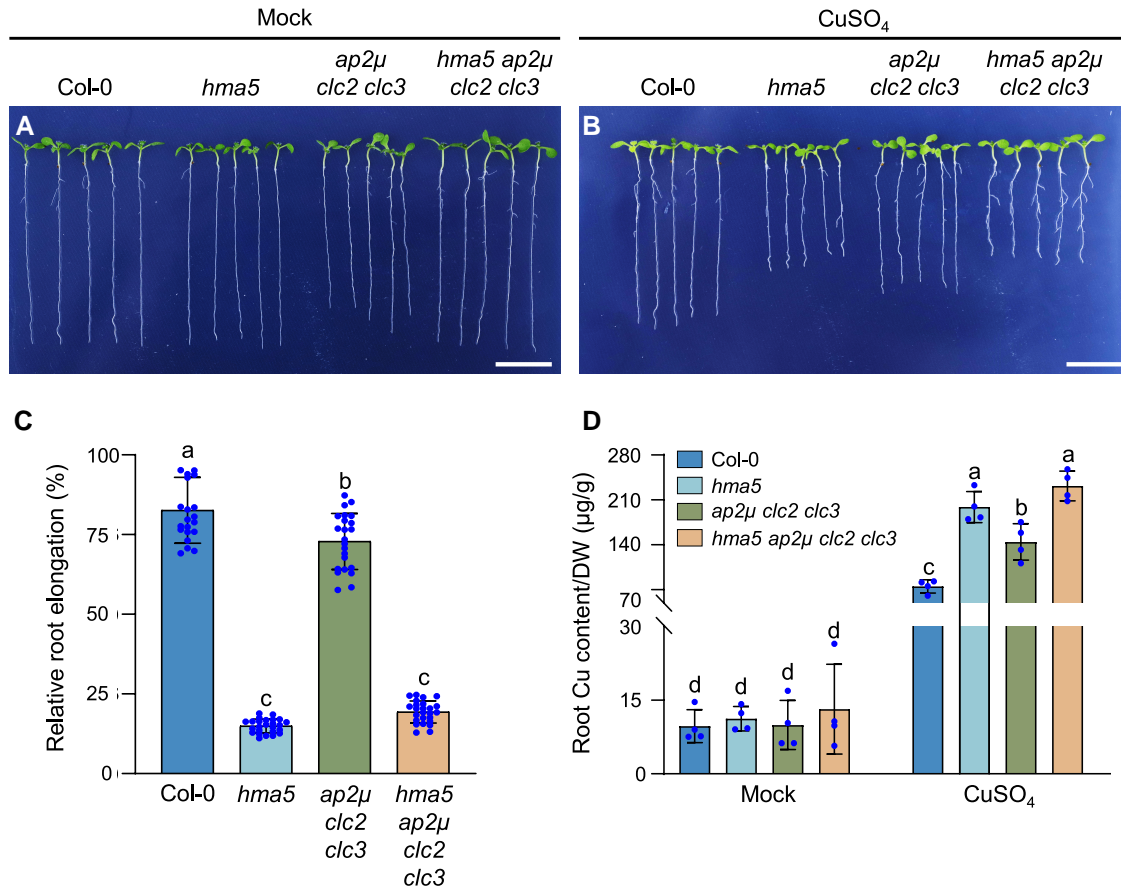
Figure 3. Clathrin regulates the copper tolerance dependent on HMA5. **A** and **B)** Five-day-old vertically grown seedlings in Col-0, *hma5*, *ap2μ clc2 clc3*, and *hma5 ap2μ clc2 clc3* mutants were transferred to 0.5× MS solid medium plates containing 0 **(A)** or 30 μM CuSO$_4$ **(B)** for 3 d. **C)** Relative root elongation under excess Cu compared with the mock controls ($n = 25$ roots from Col-0, 25 roots from *hma5*, 25 roots from *ap2μ clc2 clc3*, and 25 roots from *hma5 ap2μ clc2 clc3*). **D)** ICP-MS analysis of copper content in roots ($n = 180$ roots per experiment from four independent experiments). Shown are means $\pm$ SD. Significant differences ($P < 0.01$) are indicated by different lowercase letters above the columns (Student's t-test). Bars = 1 cm **(A** and **B)**.

previously characterized loss-of-function *ap1μ2* mutant (Park et al. 2013; Wang et al. 2013a, 2016b). We observed that the transfer of YFP-HMA5 from the TGN/EE to the PM after copper treatment was significantly attenuated in the *ap1μ2* mutant relative to that in the Col-0 (Fig. 5, O to Y), indicating that AP-1 is essential for the relocalization of HMA5 from the TGN/EE to the PM.

AP-1 complexes sort cargo proteins via recognition by the μ/σ subunit of tyrosine-based sorting (YXXΦ) or dileucine-based sorting ([DE]XXXL[LI]) motifs (Janvier et al. 2003; Carvajal-Gonzalez et al. 2012; Xu et al. 2022). Here, we found a potential tyrosine-based sorting signal, [486]YVIW[489], in the second cytoplasmic loop (Fig. 6A). To address the molecular basis for the AP-1 sorting of HMA5 at the TGN/EE, we performed yeast two-hybrid (Y2H) assays to determine the potential interaction between AP-1 and HMA5. The Y2H assay results indicated that there was interaction between AP1σ2 and HMA5, but not AP1μ2 and HMA5 (Fig. 6B). To determine whether [486]YVIW[489] is a canonical YXXΦ sorting motif, we generated a variant of the HMA5 s cytoplasmic loop (HL) carrying a Y486A/W489A double mutation (mHL). We observed a significant reduction in AP1σ2 interactions with mHL compared to HL (Fig. 6B). Bimolecular fluorescence complementation (BiFC) assays showed a significant reduction in the fluorescence signal reflecting AP1σ2 interactions with mHL compared to HL, which further demonstrated that [486]YVIW[489] is a key sorting motif for AP1σ2 binding (Fig. 6C). We performed an in vitro pull-down experiment between AP1σ2 and HL to further test whether

AP1σ2 directly interacts with HMA5. We observed that glutathione S-transferase (GST)-tagged HL, but not GST or GST-mHL, pulled down Flag-tagged AP1σ2 (Fig. 6D). Collectively, these data demonstrated that AP-1 sorts HMA5 to the PM transport pathway by recognizing the YXXΦ motif of HMA5 at the TGN/EE under Cu stress.

CMT regulates the endocytic recycling of HMA5

In plants and mammals, PM proteins are internalized and transported to the vacuole/lysosome for degradation or recycled back to the PM. This endocytic recycling mechanism determines their abundance and localization (Kleine-Vehn and Friml 2008; Hsu et al. 2012; Cullen and Steinberg 2018). Thus, we predicted that HMA5 is internalized from the PM via endocytosis after translocation from the TGN/EE, and then recycled back to the PM. We treated YFP-HMA5 transgenic seedlings in a wild-type background with the vesicle trafficking inhibitor brefeldin A (BFA), which induces the clustering of late secretory pathway compartments into BFA bodies (Geldner et al. 2003; Lam et al. 2009), in the presence of the protein synthesis inhibitor cycloheximide (CHX), which blocks de novo protein synthesis. As expected, YFP-HMA5-labeled BFA bodies were observed following 60 min of BFA treatment after 60 min of pretreatment with CuSO$_4$ and CHX (Fig. 7, A and B). In addition, YFP-HMA5 was recycled from the BFA vesicles back to the PM following BFA removal (Fig. 7C). Nevertheless, the accumulation of YFP-HMA5 in intracellular
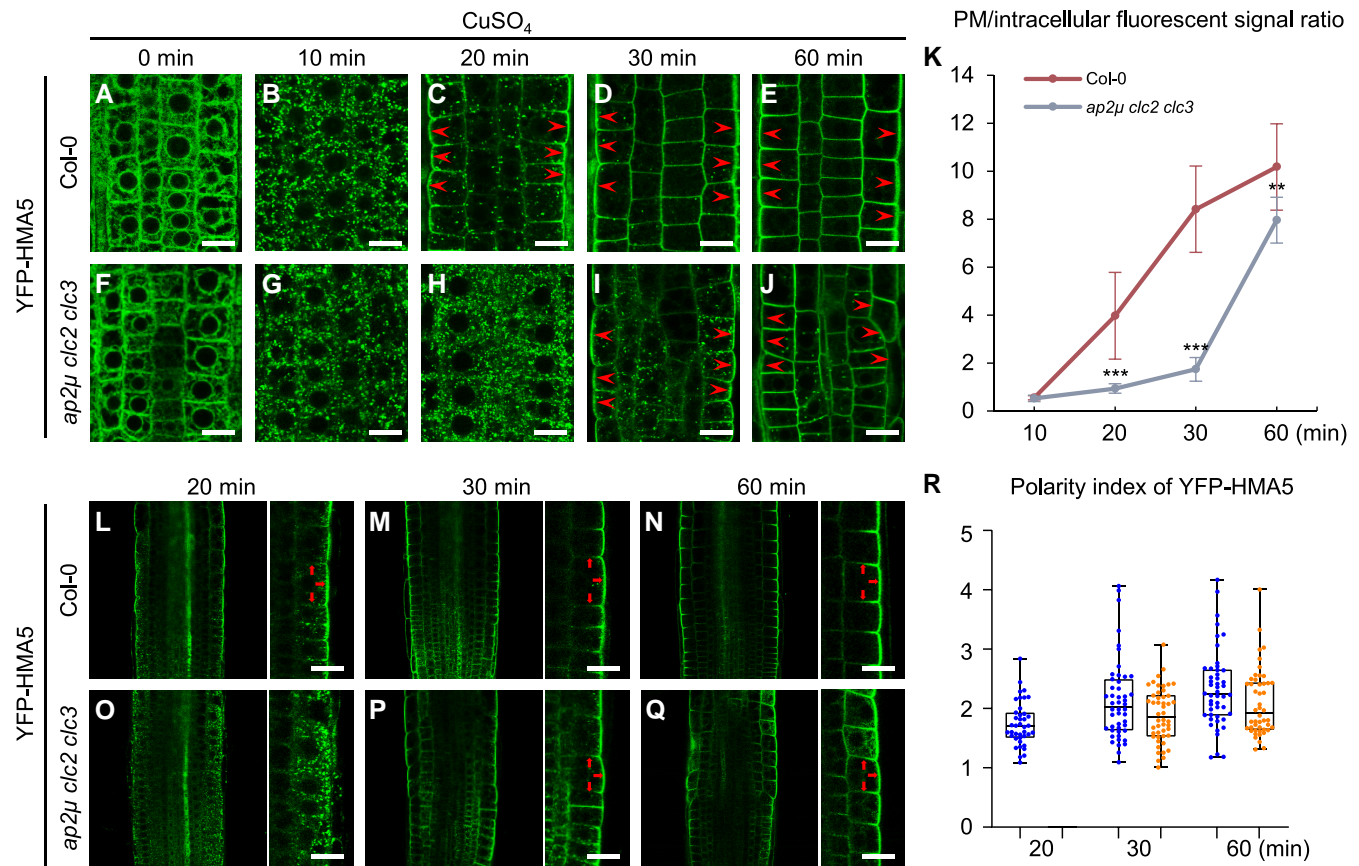
Figure 4. Impaired relocalization of YFP-HMA5 to the PM in *ap2μ clc2 clc3* mutants. **A-J)** Copper effect on localization of YFP-HMA5 in Col-0 and *ap2μ clc2 clc3* mutant root cells. **K)** Quantitative analysis of the relative ratios of the PM to intracellular fluorescent signal of YFP-HMA5 after CuSO$_4$ treatment. Different time lengths (0, 10, 20, 30, and 60 min) after addition of CuSO$_4$ (10 μM) are indicated at the top of the figure ($n = 54$ cells from 9 roots). Arrowheads in **(C)**, **(D)**, **(E)**, **(I)**, and **(J)** show PM localization of YFP-HMA5. **L-Q)** Subcellular distribution of YFP-HMA5 in Col-0 and *ap2μ clc2 clc3* mutant root epidermal cells. Different time lengths (20, 30, and 60 min) after addition of CuSO4 (10 μM) are indicated at the top of the figure. **R)** Quantitative analysis of the YFP-HMA5 polarity index ($n = 48$ cells from 6 roots). Each spot represents the data from an individual cell. Boxplots span the first to the third quartiles of the data. Whiskers indicate minimum and maximum values. A line in the box represents the mean. Arrows in **(L)**, **(M)**, **(N)**, **(P)**, and **(Q)** show PM polar localization of YFP-HMA5. Shown are means ± SD. Double and triple asterisks indicate $P < 0.01$ and 0.0001, respectively (Student's *t*-test). Bars = 10 μm **(A-J** and **L-Q)**.

BFA bodies was significantly reduced in the *ap2μ2 clc2 clc3* mutants relative to that in Col-0 (Fig. 7, B and D). Moreover, the PM recycling of internalized YFP-HMA5 from BFA bodies following BFA removal was slower in the *ap2μ2 clc2 clc3* mutants than in Col-0 (Fig. 7, C and D). These results suggested that CMT mediates the constitutive endocytic recycling of HMA5.

Studies have demonstrated that the plant adaptor protein complex AP-2 recognizes the YXXΦ or [DE]XXXL[LI] sorting motif of cargo proteins and recruits clathrin to the PM to mediate endocytosis (Kelly et al. 2008; Liu et al. 2020). Therefore, we next examined whether the abundance of AP-2 at the PM is altered in response to Cu stress. Consistent with the observed increase in CLC1 abundance at the PM following Cu treatment (Fig. 1), the levels of PM-associated AP2μ-YFP increased after CuSO$_4$ treatments for 5, 60, and 120 min relative to those of mock controls (Supplementary Fig. S10, A to G). Similarly, the PM-associated levels of AP2σ-GFP also increased after Cu exposure (Supplementary Fig. S10, H to N). To explore the mechanism underlying the regulation of HMA5 internalization by CME, we performed Y2H and BiFC assays to determine the potential for interaction between AP-2 subunits and HMA5. Similar to the AP-1 recognition of HMA5, the results of the Y2H and BiFC analysis showed that AP-2 recognizes the ^{486}YVIW^{489} sorting motif on the cytoplasmic

domain of HAM5 via the σ subunit (Fig. 7, E and F). In addition, pull-down analysis further confirmed that the key to AP2σ recognition of HMA5 lies in the binding to the ^{486}YVIW^{489} motif (Fig. 7G).

The tyrosine-based motif is necessary for the function of HMA5 in Cu detoxification

Our data indicated that the recognition of the HMA5 ^{486}YVIW^{489} tyrosine-based motif by adapter proteins AP-1 and AP-2 is essential for the CMT-mediated sorting and transport of HMA5. To verify the function of ^{486}YVIW^{489} sorting motifs in the transporter of HMA5 in response to Cu stress, we generated a variant of HMA5 carrying a Y486A/W489A double mutation (mHMA5) and constructed the UBQ10pro:YFP-mHMA5 vector. This vector was subsequently transfected into Col-0 for expression. In the presence of exogenous Cu, YFP-mHMA5 and YFP-HMA5 translocated from the ER to the TGN/EE within 10 min (Fig. 8, A, B, F, and G). However, unlike YFP-HMA5, which displayed PM localization after 20 min of copper treatment (Fig. 8C), the YFP-mHMA5 fluorescence signal was not detected at the PM (Fig. 8H). Continued exposure to Cu for 30 min was required to shift YFP-mHMA5 toward the PM (Fig. 8, D and I), and its PM abundance remained significantly lower than that of YFP-HMA5 after 60 min of copper
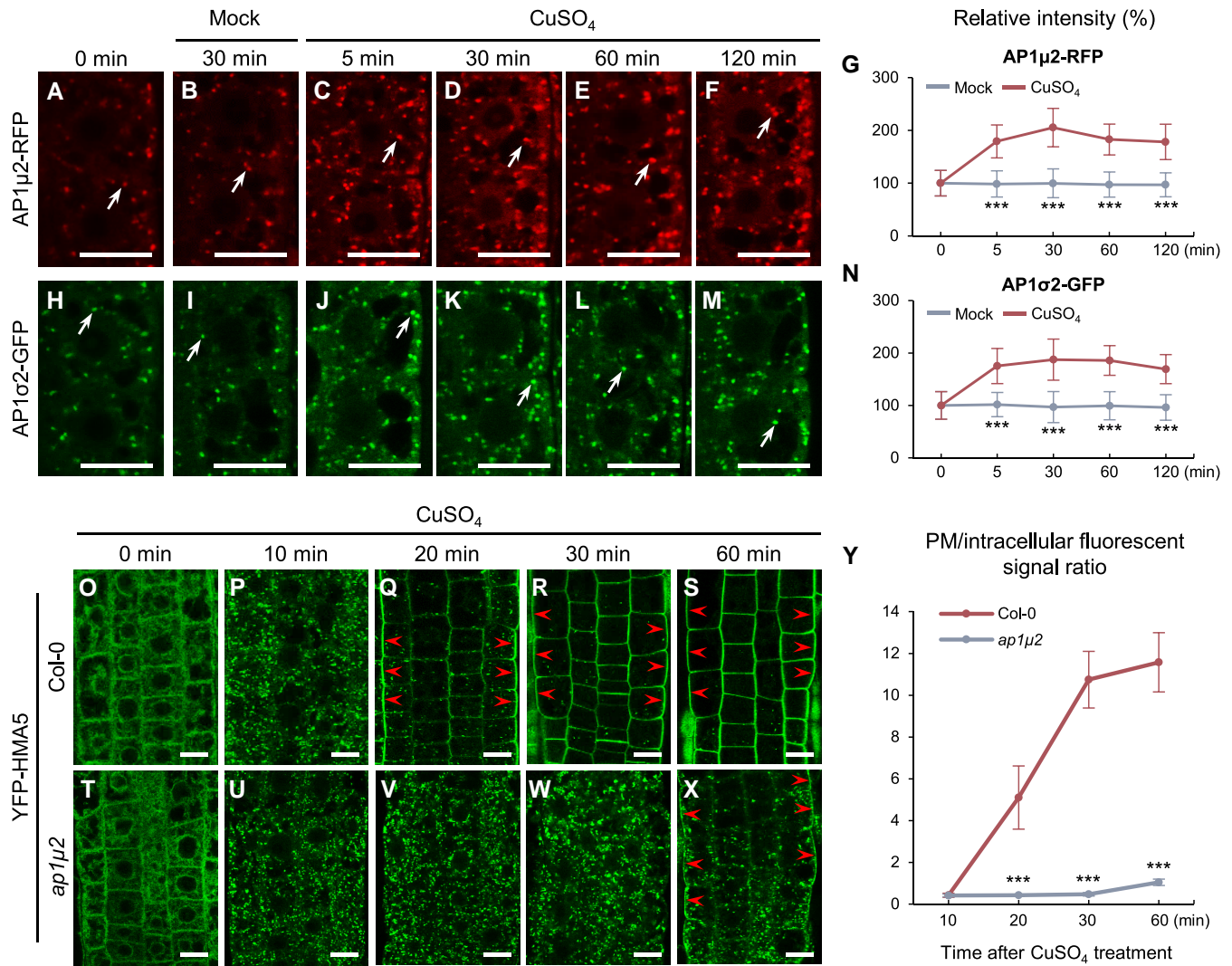
Figure 5. AP-1 mediates HMA5 translocation from the TGN/EE to PM. **A-N)** Copper effect on TGN/EE-associated AP1μ2-RFP **(A-G)** and AP1σ2-GFP **(H-N)** in the wild-type root meristem epidermal cells. **G** and **N)** The relative intensities of TGN/EE-associated AP1μ2-RFP (G) ($n = 96$ cells from 12 roots) and AP1σ2-GFP **(N)** ($n = 64$ cells from 8 roots). Different time lengths (5, 30, 60, and 120 min) after addition of $CuSO_4$ (10 μM) or in the absence of exogenous $CuSO_4$ (mock controls) are indicated at the top of the figure. **O-Y)** Copper effect on localization of YFP-HMA5 in Col-0 and *ap1μ2* mutant root cells. **Y)** Quantitative analysis of the relative ratios of the PM to intracellular fluorescent signal of YFP-HMA5 after $CuSO_4$ treatment ($n = 54$ cells from 9 roots). Different time lengths (0, 10, 20, 30, and 60 min) after the addition of $CuSO_4$ (10 μM) are indicated at the top of the figure. Arrows and arrowheads show TGN/EE-associated AP1μ2-RFP/AP1σ2-GFP or PM localization of YFP-HMA5, respectively. Shown are means ± SD. Triple asterisks indicate $P < 0.0001$ (Student's *t*-test). Bars = 10 μm **(A-F, H-M,** and **O-X).**

treatment (Fig. 8, E, J, and K). In addition, we tested the effect of [486]YVIW[489] sorting motif disruption on HMA5 endocytosis. Furthermore, there were significantly fewer YFP-mHMA5-labeled BFA bodies than YFP-HMA5-labeled BFA bodies following BFA treatment in the presence of $CuSO_4$ and CHX (Fig. 8, L, M, and O). Moreover, the rate of disappearance of YFP-mHMA5-labeled BFA bodies after BFA removal was significantly slower than that of YFP-HMA5-labeled BFA bodies (Fig. 8, N and O). These results revealed that the tyrosine-based motif is critical for HMA5 relocalization to the PM and its subsequent recycling between the TGN/EE and PM.

We next analyzed the effect of sorting motif defects on the physiological function of HMA5 as a Cu efflux transporter. Expressing YFP-HMA5 (driven by the UBQ10 promoter) in *hma5* mutants resulted in stronger resistance to copper compared with that in Col-0, while the rescue of copper sensitivity due to *hma5* loss of function was significantly weaker with YFP-mHMA5 than with YFP-HMA5 (Fig. 9, A, B, and D). Immunoblot analysis

demonstrated that the protein levels of YFP-HMA5 and YFP-mHMA5 were similar in the *hma5* mutant (Fig. 9C). Furthermore, ICP-MS analysis showed that although the Cu content in *YFP-mHMA5/hma5* roots after Cu treatment was lower than that in *hma5* roots, it was significantly higher than that in Col-0 and *YFP-HMA5/hma5* roots (Fig. 9E). These results demonstrated that the HMA5 tyrosine-based sorting signal is required for Cu tolerance.

Discussion
The role of CMT in the response of HMA5 to copper stress

CME controls the uptake of ions from the soil by regulating the PM abundance of IRT1, BOR1, and NIP5;1 in plant root cells (Barberon et al. 2011; Wang et al. 2017; Yoshinari et al. 2019). In addition to its role in CME, clathrin is also associated with the TGN/EE, while
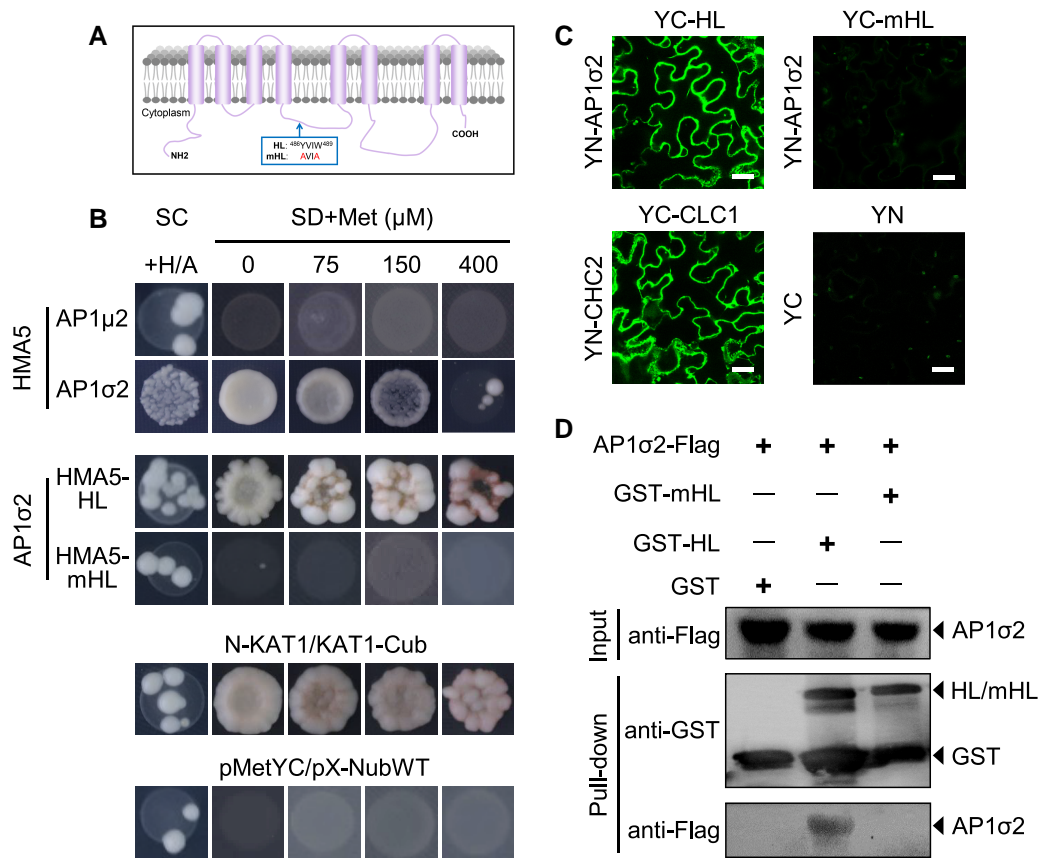
Figure 6. HMA5 tyrosine-based sorting signal interacts with AP-1 σ subunit. **A)** Predicted protein structure of RPG1. HL and mHL indicate the canonical YXXΦ sorting motif before and after mutations in the cytoplasmic loop of HMA5, respectively. **B)** Split ubiquitin Y2H (mbSUS) analysis of HMA5 interaction potential with AP1μ2 and AP1σ2. SC, synthetic complete medium; SD, synthetic defined minimal medium. pMetYC/pX-NubWT served as a negative control; N-KAT1/KAT1-Cub served as a positive control. **C)** Bimolecular fluorescence complementation (BiFC) analysis of HAM5 with AP1σ2 in *Nicotiana benthamiana* leaf epidermal cells. AP1σ2 was fused to the N-terminal part of YFP; HL and mHL were fused to the C-terminal part of YFP. CHC2-YN/CLC1-YC served as a positive control; YN/YC served as a negative control. YN, N-terminal half of YFP; YC, C-terminal half of YFP. Bar = 20 μm. **D)** In vitro pull-down analysis of interactions between AP1σ2 and HL/mHL. The AP1σ2-Flag were detected by an anti-Flag antibody. GST/GST-HL/GST-mHL were detected by an anti-GST antibody.

clathrin-dependent post-Golgi trafficking has been indicated to play an important role in cargo protein transport (Wang et al. 2013b; Yan et al. 2021).

Our results showed that once adaptor protein complex AP-1 or clathrin function is disrupted, HMA5 translocation from the TGN/EE to the PM is inhibited (Fig. 4, A to K, Fig. 5, O to Y, and Supplementary Fig. S9). This demonstrates that HMA5 is recognized as cargo by AP-1 at the TGN/EE and is subsequently translocated to the PM via the clathrin-mediated vesicular pathway. Following this, HMA5 is internalized to the cytoplasm via the CME pathway in the presence of the PM-localized adaptor protein complex AP-2 and is then either sorted at the TGN/EE for recycling to the PM or transported to the vacuole for degradation (Fig. 7, A to D and Supplementary Fig. S10; Li et al. 2017). This endocytic trafficking between the TGN/EE and the PM is likely necessary to maintain HMA5 activity. However, additional experimental evidence is required to confirm this. Notably, there is a coupling regulation between CME and clathrin-dependent post-Golgi trafficking (Yan et al. 2021). As previously reported, once AP-2/clathrin-mediated endocytosis is impaired either genetically or pharmacologically, AP-1/clathrin recruitment at the TGN/EE is reduced, thereby interfering with protein secretion (Yan et al. 2021). Thus, the slowed transport of HMA5 to the PM in the *ap2μ2 clc2 clc3* mutant (Fig. 4, A to K) was likely to have resulted from the diminished abundance of AP-1/clathrin at the TGN/EE affecting the secretory pathway, which delivers proteins to the PM. These results suggest that CMT pathways do not function in isolation but synergistically regulate protein transport in plant cells.

In addition to abundance, polarity also affects the biological function of PM proteins, while IRT1, BOR1, and NIP5;1 polarity formation is dependent on CMT (Barberon et al. 2014; Wang et al. 2017; Yoshinari et al. 2019). The disruption of the clathrin/adaptor protein or sorting motifs delayed the translocation of HMA5 from the TGN/EE to the PM, but did not affect its polar localization (Fig. 4, L to R and Fig. 8, A to K). This implies that the formation of HMA5 polarity is not dependent on CMT. However, the molecular mechanism underlying the regulation of HMA5 PM polarity remains to be elucidated.

The mechanisms involved in the CMT-mediated regulation of HMA5 localization

Cu treatment induced a rapid increase in TGN/EE-associated AP-1 and clathrin abundance within 5 min, which facilitated the transport of HMA5 to the PM for the excretion of Cu ions (Fig. 1 and Fig. 5, A to N). Moreover, there was a simultaneous increase in PM-associated AP-2 and clathrin levels to maintain the balance of HMA5 recycling between the TGN/EE and the PM through the promotion of HMA5 internalization (Fig. 1 and Supplementary Fig. S10). The relocalization of HMA5 to the PM in response to Cu
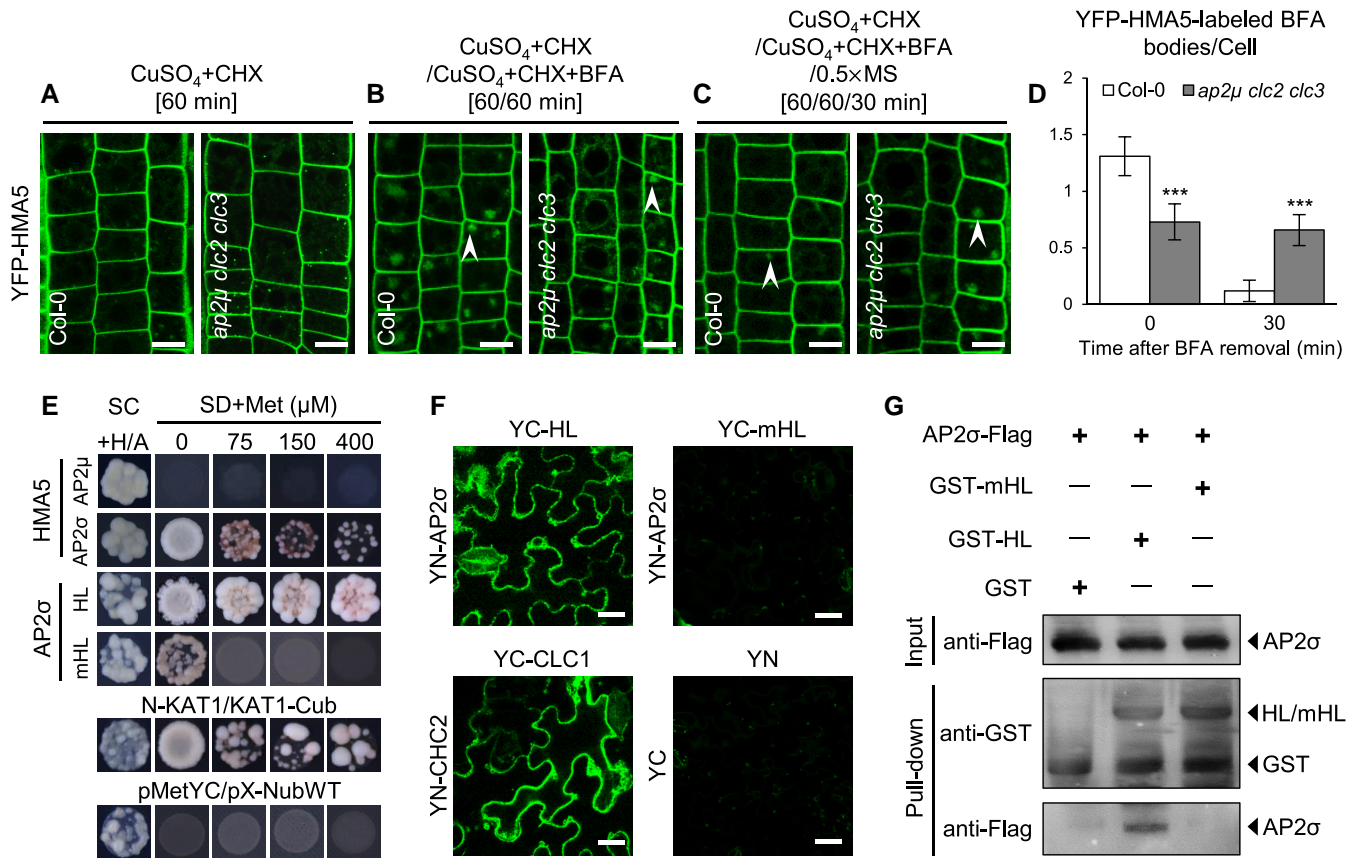
Figure 7. Reduced endocytic recycling of YFP-HMA5 in *ap2μ clc2 clc3* mutants. **A-D)** BFA-induced internalization and recycling of YFP-HMA5 in Col-0 and *ap2μ clc2 clc3* mutants. **A)** CuSO$_4$ and CHX treatments for 60 min. **B)** CuSO$_4$ and CHX pretreatments for 60 min followed by washout with CuSO$_4$, CHX, and BFA for 60 min. **C)** The seedlings were pretreated with CuSO$_4$ and CHX for 60 min, followed by washout with CuSO$_4$, CHX, and BFA for 60 min, and finally by washout with 0.5× MS liquid media for 30 min in Col-0 and *ap2μ clc2 clc3* before CLSM imaging. **D)** The average number of YFP-HMA5-labeled BFA bodies (*n* = 144 cells from 12 roots). **E)** Split ubiquitin Y2H (mbSUS) analysis of HMA5 interaction potential with AP2μ and AP2σ. SC, synthetic complete medium; SD, synthetic defined minimal medium. pMetYC/pX-NubWT served as a negative control; N-KAT1/KAT1-Cub served as a positive control. **F)** BiFC analysis of HAM5 with AP2σ in *Nicotiana benthamiana* leaf epidermal cells. AP2σ was fused to the N-terminal part of YFP; HL and mHL were fused to the C-terminal part of YFP. CHC2-YN/CLC1-YC served as a positive control; YN/YC served as a negative control. **G)** In vitro pull-down analysis of interactions between AP2σ and HL/mHL. The AP2σ-Flag were detected by an anti-Flag antibody. GST/GST-HL/GST-mHL were detected by an anti-GST antibody. Arrowheads show YFP-HMA5-labeled BFA bodies. Shown are means ± SD. Triple asterisks indicate *P* < 0.0001 (Student's *t*-test). Bars = 10 (A, B, C) or 20 μm **(F)**.

stress in the *ap2μ2 clc2 clc3* mutant was significantly slower than that of the wild type (Fig. 4, A to K), which may explain its deeper Cu toxicity (Fig. 2). Similarly, we observed that a mutation in the HMA5 sorting motif suppressed PM transfer and enhanced the sensitivity of plants to copper (Fig. 8, A to K and Fig. 9). These data suggest that the rate of translocation of HMA5 to the PM in response to external Cu concentrations is positively associated with Cu resistance in plants. Accordingly, exploring the rapid response mechanism involved in CMT-mediated regulation of HMA5 localization is key to understanding Cu tolerance in plants.

Protein phosphorylation plays a key role in many biological processes as well as in responses to environmental cues (Zhang et al. 2023). Moreover, tyrosine phosphorylation has recently been shown to be involved in plant responses to environmental changes via the regulation of signal transduction (Song et al. 2022). Our results revealed the critical role of the HMA5 tyrosine-based sorting motif in the CMT-mediated transport of HMA5 under Cu stress. The absence of sorting signals affects the relocalization of HMA5 in response to Cu stress and prevents HMA5 from contributing to increased Cu tolerance in plants (Fig. 8, L to O and Fig. 9). To determine whether Y486 in the sorting motif affects HMA5 phosphorylation, we evaluated the phosphorylation levels

of YFP-HMA and YFP-mHMA5. As shown in Supplementary Fig. S11, no significant difference in phosphorylation levels was detected between YFP-HMA and YFP-mHMA5, indicating that Y486 phosphorylation is not required for the regulation of HMA5 transport. However, whether plants regulate CMT in response to Cu stress to mediate HMA5 translocation through protein phosphorylation requires further investigation.

Materials and methods
Plant materials and growth conditions

All *Arabidopsis thaliana* materials used in this study were authorized and were of the Columbia-0 (Col-0) background. The following transgenic lines and mutants were used in this study: transgenic lines 35Spro:CLC1-GFP (Wang et al. 2013b); AP1μ2pro: AP1μ2-RFP (Wang et al. 2013a); 35Spro:AP1σ2-GFP (Yan et al. 2021); AP2μpro:AP2μ-YFP (Bashline et al. 2013); AP2σpro: AP2σ-GFP (Fan et al. 2013); CLC2pro:CLC2-mKO (Ito et al. 2012); VHAa1pro:VHAa1-RFP (Dettmer et al. 2006); SNX1Pro:SNX1-RFP (Ambrose et al. 2013); UBQ10pro:YFP-HMA5 (this study); *clc2* (SALK_016049; Wang et al. 2013b); *clc3* (CS100219; Wang et al.
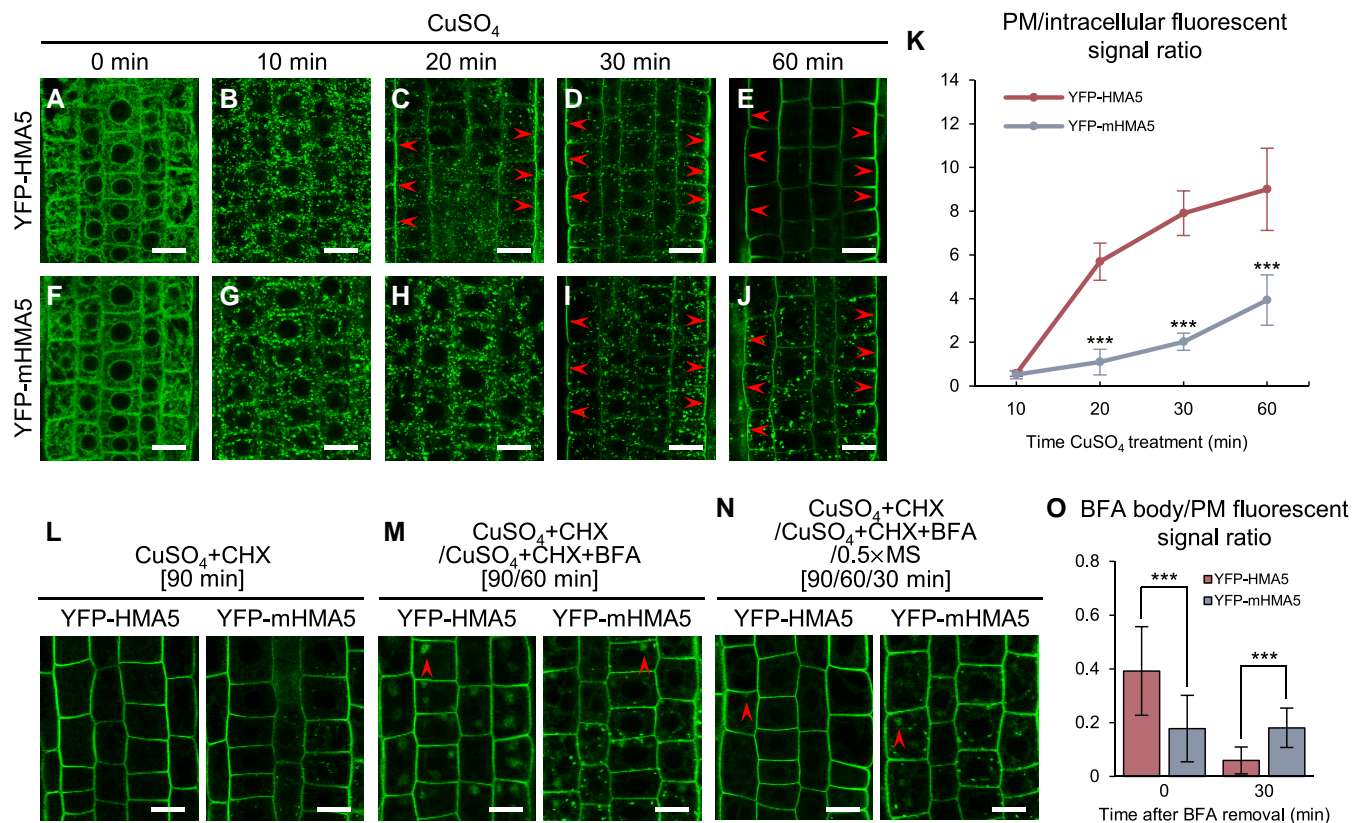
Figure 8. Tyrosine-based sorting signal is required for HMA5 trafficking between TGN/EE and PM. **A-J)** Copper effect on localization of YFP-HMA5 and YFP-mHMA5 in Col-0 root cells. **K)** Quantitative analysis of the relative ratios of the PM to intracellular fluorescent signal of YFP-HMA5 and YFP-mHMA5 after CuSO$_4$ treatment ($n = 54$ cells from 9 roots). Different time lengths (0, 10, 20, 30, and 60 min) after the addition of CuSO$_4$ (10 μM) are indicated at the top of the figure. **L-O)** BFA-induced internalization and recycling of YFP-HMA5 and YFP-mHMA5 in Col-0. **L)** CuSO$_4$ and CHX treatments for 90 min. **M)** CuSO$_4$ and CHX pretreatments for 90 min followed by washout with CuSO$_4$, CHX, and BFA for 60 min. **N)** The seedlings were pretreated with CuSO$_4$ and CHX for 90 min, followed by washout with CuSO$_4$, CHX, and BFA for 60 min, and finally by washout with 0.5× MS liquid media for 30 min before CLSM imaging. **O)** Quantitative analysis of the ratios of the BFA body to PM fluorescent signal of YFP-HMA5 and YFP-mHMA5 ($n = 192$ cells from 16 roots). Arrowheads show PM localization of YFP-HMA5/YFP-mHMA5 **(C, D, E, I, J)** or YFP-HMA5/YFP-mHMA5-labeled BFA bodies **(M, N)**, respectively. Shown are means ± SD. Triple asterisks indicate $P < 0.0001$ (Student's *t*-test). Bars = 10 μm **(A-J** and **L-N)**.

2013a); *ap1μ2* (CS16318; Yan et al. 2021); *ap2μ* (SALK_083693C; Wang et al. 2016a); *hma5* (SALK_040252 from ABRC; Li et al. 2017); *copt1* (SALK_017507C from ABRC); *copt2* (SALK_147451C from ABRC); *zip2* (SALK_094937C from ABRC); and *zip4* (SALK_145371C from ABRC).

UBQ10pro:YFP-HMA5 was constructed using PCR, restriction enzyme digestion, and ligation into transformation vectors. Sequences of primers used for cloning are listed in Supplementary Table S1. The HMA5 coding sequence harboring two point mutations (HMA5$^{Y486A/W489A}$) was generated using UBQ10pro:YFP-HMA5 as a template for site-directed mutagenesis with the primers listed in Supplementary Table S1. As AtHMA5 is toxic to *Escherichia coli*, the recombination products were transformed into the *Agrobacterium tumefaciens* strain GV3101 by electroporation. The transformation of *A. thaliana* plants was conducted by floral dip (Clough and Bent 1998). Homozygous mutant lines, including *clc* (Wang et al. 2013b), *ap-1* (Yan et al. 2021), and *ap-2* (Fan et al. 2013; Wang et al. 2016b), were isolated and identified by PCR-based assays. The *clc2 clc3*, *ap2μ clc2 clc3*, *hma5 ap2μ clc2 clc3*, and *copt1 ap2μ clc2 clc3* multiple mutants were generated by crossing, and verified by genotyping PCR. Fluorescently tagged marker lines (CLC2pro:CLC2-mKO, VHAa1pro:VHAa1-RFP, and SNX1Pro:SNX1-RFP) were crossed into UBQ10pro:YFP-HMA5; UBQ10pro:YFP-HMA5 was crossed into *ap1μ2*, *ap2μ clc2 clc3*, and *hma5*. Homozygous lines were

confirmed based on their mutant phenotypes, genotyping PCR (Supplementary Table S2), and fluorescence.

Seeds were surface-sterilized and stratified for 3 d at 4 °C in the dark and sown onto 1/2 MS medium with 1.5% (w/v) agar unless otherwise specified. Seedlings were grown vertically on plates in a climate-controlled growth room (22 °C/20 °C day/night temperature, 16-h/8-h light/dark photoperiod, and 80 μE s^{-1} m^{-2} light intensity). For the CuSO$_4$ treatment assay, 5-day-old seedlings were transferred to 1/2 MS medium with or without 30/50 μM CuSO$_4$ 5H$_2$O (Sinopharm, Catalog No.20210408) for 3 d before being scored and photographed.

Hydroponic conditions and Cu elemental analysis

After opening the pores, the brown centrifuge tube cover was cut and germination medium containing 0.8% agar was injected inside. The brown centrifuge tube cover was then placed on a 500-mL centrifugal tube box. Following this, 1/8 MS liquid medium containing 2.5 or 5 μM CuSO$_4$ 5H$_2$O was added to several boxes. The Col-0 and *ap2μ clc2 clc3* seeds that underwent vernalization were placed on germination medium and left to cultivate in a greenhouse for 15 d to observe the growth status of the main roots of Arabidopsis seedlings.

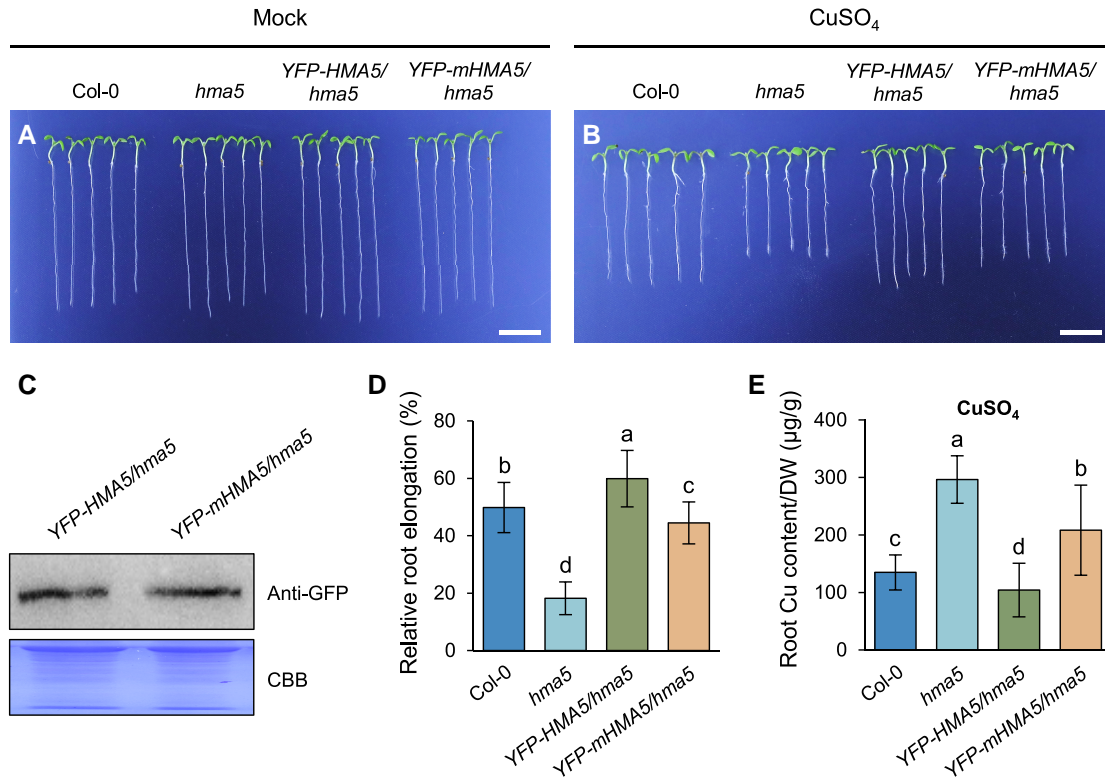Cu content was determined in 8-day-old wild-type and mutant seedlings previously washed once with 10 mM EDTA and three

Figure 9. HMA5 tyrosine-based sorting signal is required for copper tolerance. **A** and **B)** Five-day-old vertically grown seedlings in Col-0, *hma5*, *UBQ10pro:YFP-HMA5/hma5*, and *UBQ10pro:YFP-mHMA5/hma5* were transferred to 0.5× MS solid medium plates containing 0 **(A)** or 50 μM CuSO$_4$ **(B)** for 3 d. **C)** Immunoblot analysis of the levels of YFP-HMA5 and YFP-mHMA5 in total protein extracts from 5-day-old *YFP-HMA5/hma5* and *YFP-mHMA5/hma5* seedlings, respectively. **D)** Relative root elongation under excess Cu compared with the mock controls ($n = 60$ roots). **E)** ICP-MS analysis of copper content in roots after CuSO$_4$ treatment. mHMA5 indicates HMA5$^{Y486A/W489A}$ mutation ($n = 180$ roots per experiment from six independent experiments). Shown are means ± SD. Significant differences ($P < 0.001$) are indicated by different lowercase letters above the columns (Student's *t*-test). Bars = 1 cm **(A** and **B)**.

times with deionized water. The samples were completely dried in an oven at 65 °C for 1 d to calculate the dried weight. Following this, the plant samples were digested in pure nitric acid solution at 120 °C for 3 h and 150 °C for 1 h. The samples were dissolved in deionized water and analyzed via ICP-MS (iCAP RQ, Thermo Fisher Scientific, USA).

Chemical solutions and treatments

All reagents were obtained from Sigma-Aldrich (USA) unless otherwise specified. Dimethyl sulfoxide (DMSO, Sinopharm, China, Catalog No. 20231012) was used to dissolve BFA (50 mM stock), ES9 (10 mM stock), and CHX (50 mM stock). Unless otherwise indicated, the final working concentrations were 1 μM for ES9 and 50 μM for CHX and BFA. CuSO$_4$ 5H$_2$O was prepared as a 20-mM stock solution in H$_2$O and used at the indicated concentrations for the different experiments. All pre- and post-treatment durations are indicated in the text. Unless otherwise specified, pretreatments and treatments for subcellular localization analysis of membrane-associated proteins were performed in liquid medium (1/2 MS basal salts, 1% Suc, 0.05% MES [w/v], and pH 5.6 to 5.8).

Immunofluorescence analysis and live-cell CLSM

Immunolocalization analysis was performed as previously described (Wang et al. 2013b, 2016a). All primary antibodies used for immunolocalization were detected using Cy3-labeled anti-rabbit secondary antibodies (1:100 dilution; Sigma-Aldrich,

USA, Catalog No. C2306). Images were captured using a confocal laser scanning microscope (Leica Stellaris 5). For the imaging of Cy3, the 560 nm line of a helium/neon laser was used for excitation, and emission was detected from 570 to 590 nm. For the live-cell imaging of GFP and YFP, the 488- and 514-nm lines of an argon laser were used for excitation, and emissions were detected in the ranges of 496 to 532 and 520 to 560 nm, respectively. For the imaging of mKO and RFP, the 543- and 594-nm lines of the helium/neon laser were used for excitation, and emissions were detected in the ranges of 560 to 600 and 612 to 666 nm, respectively.

For quantitative fluorescence measurements, the confocal microscope parameters (laser power, 2% to 4%; pinhole, 1.0; gain value, 40) were kept identical among treatments and genotypes. To quantify the intensity of fluorescence signals at the PM or intracellular compartments, digital images of root epidermal cells within the division/transition zone were analyzed using ImageJ (http://rsb.info.nih.gov/ij/). Further details of the quantification methods are described in previous studies (Wang et al. 2013b, 2016a; Yan et al. 2021). To quantify the polarity index of YFP-HMA5, the apical and basal domains of the PM in epidermal cells in the meristematic and transition zones were selected using the segmented line tool and quantified using ImageJ. The fluorescent signal of the soil side was divided based on the stele side (Fig. 4). To measure the BFA-induced internalization of PM-localized proteins, the levels of internalized GFP-fused PM proteins were calculated as the average number of fluorescence-labeled BFA bodies per cell (Wang et al. 2013b).

Reverse transcription-quantitative PCR assays

Total RNA was isolated using a FastPure Universal Plant Total RNA Isolation Kit (Vazyme, China, Catalog No. RC411-01). Reverse transcription was performed using the HiScript III 1st Strand cDNA Synthesis Kit (+Gdna wiper) (Vazyme, Catalog No. R312-02). The resulting cDNA was used as a template for the PCR amplification for *CLC1*, *CLC2*, *CLC3*, and *HMA5* using gene-specific primers. *qUBI7* served as the internal control. The CFX 96 C1000 Thermal Cycler (Bio-Rad, USA) was used for qPCR, and Bio-Rad CFX Manager v.3.1 was used for the analysis of expression levels using the $2^{-\Delta\Delta Cq}$ method. The qPCR assay was performed as described previously (Wang et al. 2016a). Primer sequences are shown in Supplementary Table S3.

Yeast two-hybrid assay

A mating-based split ubiquitin Y2H system (mbSUS) (Obrdlik et al. 2004) was used to test interactions of AP2σ, AP2μ2, AP1σ2, and AP1μ2 with HMA5. The full-length coding sequences of AP2σ, AP2μ2, AP1σ2, and AP1μ2 were PCR-amplified and mixed with linearized pX-NubWTgate vectors to transform yeast strain THY.AP5 through in vivo DNA recombination. Full-length coding sequences of HMA5, the second cytoplasmic loops of HMA5 (HL), and HL$^{Y486A/W489A}$ (mHL) were PCR-amplified and mixed with linearized pMetYCgate vectors to transform yeast strain THY.AP4 through in vivo DNA recombination. Diploid cells were selected on synthetic complete medium containing adenine and histidine (SC + Ade + His), and interactions were tested by spotting colonies onto synthetic defined minimal medium (SD) plates containing 0, 75, 150, or 400 μM methionine. pMetYC and pX-NubWT were used as negative controls and KAT1 (as N-KAT1 and KAT-Cub) was used as a positive control. Sequences of primers used for cloning are listed in Supplementary Table S1.

Bimolecular fluorescence complementation assays

For the BiFC assays, the full-length coding sequences of AP1σ2 and AP2σ were individually cloned in-frame with the N-terminal half of the YFP sequence in the vector pEarlygate201-YN. The second cytoplasmic loops of HMA5 (HL) and HL$^{Y486A/W489A}$ (mHL) were cloned in-frame with the C-terminal half of YFP in pEarOleygate202-YC. These constructs were introduced into the *Agrobacterium tumefaciens* strain GV3101 and co-infiltrated into young leaves of *Nicotiana benthamiana* plants grown for approximately 3 wks. YFP fluorescence was measured using CLSM (Stellaris 5, Leica, Germany) after 48 h. Arabidopsis CHC2-YN and CLC1-YC were used as the positive control. Constructs expressing YFP-N (YN) and YFP-C (YC) were used as the negative control. Sequences of primers used for cloning are listed in Supplementary Table S1.

Pull-down assay

The in vitro pull-down assay was performed as previously described (Zhang et al. 2021). To detect the interaction of AP1σ and AP2σ with HL1, the coding sequences of AP1σ, AP2σ, HL1, and mHL1 were cloned into pCDF-duet-1 (Flag-tagged) and pGEX-4T-1 (GST-tagged). The recombinant vectors were separately transferred into the BL21 strain. Extracts from bacteria expressing GST or GST-HL1/mHL1 were incubated with glutathione Sepharose (GE Healthcare, USA) for 60 min at room temperature in a binding buffer (50 mM Tris of pH 7.4, 120 mM NaCl, 5% glycerol, 0.5% NonidetP-40, 1 mM phenylmethanesulfonyl fluoride, and 1 mM β-mercaptoethanol). The resins were then collected for further incubation with extracts from bacteria expressing AP1σ-FLAG or AP2σ-FLAG at room temperature for 60 min. After rinsing five times with washing buffer (50 mM Tris, pH 7.4, 120 mM NaCl, 5% glycerol, and 0.5% Nonidet P-40), the Sepharose was mixed with SDS sample buffer and boiled for SDS/PAGE and immunoblotting. Sequences of primers used for cloning are listed in Supplementary Table S1.

Immunoblot analysis

Total protein fractions were prepared as previously described (Wang et al. 2016a). For immunoblot analysis, an anti-GFP antibody (1:5000 dilution; TransGen Biotech, China, Catalog No. HT801) was used. Coomassie brilliant blue (CBB) staining served as a loading control. The primary antibody was detected using an anti-mouse secondary antibody (1:50,000 dilution; HUABIO, China, Catalog No. HA1009) conjugated to horseradish peroxidase and detected using an enhanced chemiluminescence substrate (Thermo Scientific).

Phosphorylation assay

To analyze the phosphorylation of the YFP-tagged HMA5 and mHMA5 proteins, 6-day-old transgenic plants expressing the corresponding YFP fusions were freeze-dried, ground to a powder, and homogenized in 1 mL of IP buffer (10 mM Tris-HCl of pH 7.4, 100 mM NaCl, 10% glycerol, 0.5% NP-40, and 1× protease inhibitor and PhosSTOP Phosphatase Inhibitor cocktail). Lysates were clarified by centrifugation at 12,000 rpm for 30 min at 4 °C and were immunoprecipitated with GFP-Trap (ChromoTek, USA). After incubation, the beads were washed three times with ice-cold washing buffer (10 mM Tris-HCl of pH 7.4, 100 mM NaCl, 10% glycerol) and then eluted by boiling in reducing SDS sample buffer. Samples were subjected to SDS/PAGE and immunoblotting using an anti-phosphoserine antibody (1:500 dilution; HUABIO, China, Catalog No. ET1704-20). In addition, to observe the total quantities of immunoprecipitated GFP-fused proteins used for Phos-tag detection, the same quantities of immunoprecipitated proteins from each sample were also separated by SDS/PAGE followed by western blotting analysis with an anti-GFP antibody (1:5000 dilution; TransGen Biotech, China, Catalog No. HT801). Chemiluminescence was imaged using a ChemiDoc imaging system (Bio-Rad).

Statistical analysis

All experiments were independently performed at least three times and statistical significance was evaluated using Student's *t*-tests (paired with two-tailed distribution) or one-way analysis of variance (ANOVA). Statistical analyses were performed using GraphPad Prism for Windows (64-bit, v.8.4.0) and Microsoft Excel 2019.

Accession numbers

Sequence data from this manuscript can be found in the Arabidopsis Genome Initiative under the following accession numbers: *CLC1* (At2g20760), *CLC2* (At2g40060), *CLC3* (At3g51890), *CHC2* (At3g08530), *AP1σ2* (At2g17380), *AP1μ2* (At1g60780), *AP2σ* (At1g47830), *AP2μ* (At5g46630), *VHAa1* (At2g28520), *SNX1* (AT5G06140), *HMA5* (AT1G63440), *COPT1* (AT5G59030), *COPT2* (AT3G46900), *ZIP2* (AT5G59520), *ZIP4* (AT1G10970), and *UBIQUITIN 7* (At2g35635).

Author contributions

L.W., M.X., X.Y., J.S., and C.W. conceived the study and designed the experiments. L.W., M.X., Y.S., G.Z., Y.R., H.L., J.M., J.J., X.C., X.Y., J.S., and C.W. carried out the experiments. L.W., M.X., X.Y., J.S., and C.W. analyzed the data. L.W., M.X., X.Y., J.S., and C.W. wrote the article.

Supplementary data

The following materials are available in the online version of this article.

Supplementary Figure S1. CLSM Imaging of membrane-associated CLC1-GFP in root cells upon exposure to magnesium, zinc, or iron.

Supplementary Figure S2. RT-qPCR analysis of the transcription levels of *CLCs*.

Supplementary Figure S3. Immunoblot analysis of the levels of CLC1-GFP.

Supplementary Figure S4. Analysis of Cu tolerance in Cu transporter function-deficient mutants.

Supplementary Figure S5. Impaired Cu efflux in *ap2μ clc2 clc3* mutant roots.

Supplementary Figure S6. ICP-MS analysis of Cu content in seedling shoots.

Supplementary Figure S7. RT-qPCR analysis of *HMA5* transcription levels.

Supplementary Figure S8. YFP-HMA5 colocalized preferentially with TGN/EE proteins.

Supplementary Figure S9. The effects of the CHC function inhibitor ES9 on YFP-HMA5 relocalization.

Supplementary Figure S10. Cu Enhanced the localization of AP-2 subunits to the plasma membrane.

Supplementary Figure S11. Phosphorylation assay for YFP-HMA5 and YFP-mHMA5 proteins.

Supplementary Table S1. PCR Primer sequences for cloning.

Supplementary Table S2. PCR Primer sequences for genotyping.

Supplementary Table S3. PCR Primer sequences for RT-qPCR.

Funding

Data availability

The data underlying this article are available in the article and in its online supplementary material.

References

Ambrose C, Ruan Y, Gardiner J, Tamblyn LM, Catching A, Kirik V, Marc J, Overall R, Wasteneys GO. CLASP interacts with sorting nexin 1 to link microtubules and auxin transport via PIN2 recycling in *Arabidopsis thaliana*. *Dev Cell.* 2013:24(6):649–659. https://doi.org/10.1016/j.devcel.2013.02.007

Andrés-Colás N, Perea-García A, Puig S, Peñarrubia L. Deregulated copper transport affects Arabidopsis development especially in the absence of environmental cycles. *Plant Physiol.* 2010:153(1):170–184. https://doi.org/10.1104/pp.110.153676

Andrés-Colás N, Sancenón V, Rodríguez-Navarro S, Mayo S, Thiele DJ, Ecker JR, Puig S, Peñarrubia L. The Arabidopsis heavy metal P-type ATPase HMA5 interacts with metallochaperones and functions in copper detoxification of roots. *Plant J.* 2006:45(2):225–236. https://doi.org/10.1111/j.1365-313X.2005.02601.x

Barberon M, Dubeaux G, Kolb C, Isono E, Zelazny E, Vert G. Polarization of IRON-REGULATED TRANSPORTER 1 (IRT1) to the plant-soil interface plays crucial role in metal homeostasis. *Proc Natl Acad Sci U S A.* 2014:111(22):8293–8298. https://doi.org/10.1073/pnas.1402262111

Barberon M, Zelazny E, Robert S, Conéjéro G, Curie C, Friml J, Vert G. Monoubiquitin-dependent endocytosis of the iron-regulated transporter 1 (IRT1) transporter controls iron uptake in plants. *Proc Natl Acad Sci U S A.* 2011:108(32):E450–E458. https://doi.org/10.1073/pnas.1100659108

Bashline L, Li S, Anderson CT, Lei L, Gu Y. The endocytosis of cellulose synthase in Arabidopsis is dependent on μ2, a clathrin-mediated endocytosis adaptin. *Plant Physiol.* 2013:163(1):150–160. https://doi.org/10.1104/pp.113.221234

Burkhead JL, Reynolds KAG, Abdel-Ghany SE, Cohu CM, Pilon M. Copper homeostasis. *New Phytol.* 2009:182(4):799–816. https://doi.org/10.1111/j.1469-8137.2009.02846.x

Carvajal-Gonzalez JM, Gravotta D, Mattera R, Diaz F, Bay AP, Roman AC, Schreiner RP, Thuenauer R, Bonifacino JS, Rodriguez-Boulan E. Basolateral sorting of the coxsackie and adenovirus receptor through interaction of a canonical YXXΦ motif with the clathrin adaptors AP-1A and AP-1B. *Proc Natl Acad Sci U S A.* 2012:109(10):3820–3825. https://doi.org/10.1073/pnas.1117949109

Chen G, Li J, Han H, Du R, Wang X. Physiological and molecular mechanisms of plant responses to copper stress. *Int J Mol Sci.* 2022:23(21):12950. https://doi.org/10.3390/ijms232112950

Clough SJ, Bent AF. Floral dip: a simplified method for Agrobacterium-mediated transformation of *Arabidopsis thaliana.* *Plant J.* 1998:16(6):735–743. https://doi.org/10.1046/j.1365-313x.1998.00343.x

Cullen PJ, Steinberg F. To degrade or not to degrade: mechanisms and significance of endocytic recycling. *Nat Rev Mol Cell Biol.* 2018:19(11):679–696. https://doi.org/10.1038/s41580-018-0053-7

Dejonghe W, Sharma I, Denoo B, De Munck S, Lu Q, Mishev K, Bulut H, Mylle E, De Rycke R, Vasileva M, *et al.* Disruption of endocytosis through chemical inhibition of clathrin heavy chain function. *Nat Chem Biol.* 2019:15(6):641–649. https://doi.org/10.1038/s41589-019-0262-1

Dettmer J, Hong-Hermesdorf A, Stierhof YD, Schumacher K. Vacuolar H$^+$-ATPase activity is required for endocytic and secretory trafficking in Arabidopsis. *Plant Cell.* 2006:18(3):715–730. https://doi.org/10.1105/tpc.105.037978

Fan L, Hao H, Xue Y, Zhang L, Song K, Ding Z, Botella MA, Wang H, Lin J. Dynamic analysis of Arabidopsis AP2 σ subunit reveals a key role in clathrin-mediated endocytosis and plant development. *Development.* 2013:140(18):3826–3837. https://doi.org/10.1242/dev.095711

Festa RA, Thiele DJ. Copper: an essential metal in biology. *Curr Biol.* 2011:21(21):R877–R883. https://doi.org/10.1016/j.cub.2011.09.040

Gadeyne A, Sánchez-Rodríguez C, Vanneste S, Di Rubbo S, Zauber H, Vanneste K, Van Leene J, De Winne N, Eeckhout D, Persiau G, *et al.* The TPLATE adaptor complex drives clathrin-mediated endocytosis in plants. *Cell.* 2014:156(4):691–704. https://doi.org/10.1016/j.cell.2014.01.039

Geldner N, Anders N, Wolters H, Keicher J, Kornberger W, Muller P, Delbarre A, Ueda T, Nakano A, Jürgens G. The Arabidopsis

GNOM ARF-GEF mediates endosomal recycling, auxin transport, and auxin-dependent plant growth. *Cell*. 2003:112(2):219–230. https://doi.org/10.1016/S0092-8674(03)00003-5

Grones P, De Meyer A, Pleskot R, Mylle E, Kraus M, Vandorpe M, Yperman K, Eeckhout D, Dragwidge JM, Jiang Q, *et al*. The endocytic TPLATE complex internalizes ubiquitinated plasma membrane cargo. *Nat Plants*. 2022:8(12):1467–1483. https://doi.org/10.1038/s41477-022-01280-1

Hsu VW, Bai M, Li J. Getting active: protein sorting in endocytic recycling. *Nat Rev Mol Cell Biol*. 2012:13(5):323–328. https://doi.org/10.1038/nrm3332

Ito E, Fujimoto M, Ebine K, Uemura T, Ueda T, Nakano A. Dynamic behavior of clathrin in *Arabidopsis thaliana* unveiled by live imaging. *Plant J*. 2012:69(2):204–216. https://doi.org/10.1111/j.1365-313X.2011.04782.x

Janvier K, Kato Y, Boehm M, Rose JR, Martina JA, Kim BY, Venkatesan S, Bonifacino JS. Recognition of dileucine-based sorting signals from HIV-1 Nef and LIMP-II by the AP-1γ-σ1 and AP-3 deltaδ-σ3 hemicomplexes. *J Cell Biol*. 2003:163(6):1281–1290. https://doi.org/10.1083/jcb.200307157

Kaksonen M, Roux A. Mechanisms of clathrin-mediated endocytosis. *Nat Rev Mol Cell Biol*. 2018:19(5):313–326. https://doi.org/10.1038/nrm.2017.132

Kelly BT, McCoy AJ, Späte K, Miller SE, Evans PR, Höning S, Owen DJ. A structural explanation for the binding of endocytic dileucine motifs by the AP2 complex. *Nature*. 2008:456(7224):976–979. https://doi.org/10.1038/nature07422

Kim SY, Xu ZY, Song K, Kim DH, Kang H, Reichardt I, Sohn EJ, Friml J, Juergens G, Hwang I. Adaptor protein complex 2-mediated endocytosis is crucial for male reproductive organ development in Arabidopsis. *Plant Cell*. 2013:25(8):2970–2985. https://doi.org/10.1105/tpc.113.114264

Kleine-Vehn J, Friml J. Polar targeting and endocytic recycling in auxin-dependent plant development. *Annu Rev Cell Dev Biol*. 2008:24(1):447–473. https://doi.org/10.1146/annurev.cellbio.24.110707.175254

Kobayashi Y, Kuroda K, Kimura K, Southron-Francis JL, Furuzawa A, Kimura K, Iuchi S, Kobayashi M, Taylor GJ, Koyama H. Amino acid polymorphisms in strictly conserved domains of a P-type ATPase HMA5 are involved in the mechanism of copper tolerance variation in Arabidopsis. *Plant Physiol*. 2008:148(2):969–980. https://doi.org/10.1104/pp.108.119933

Lam SK, Cai Y, Tse YC, Wang J, Law AHY, Pimpl P, Chan HYE, Xia J, Jiang L. BFA-induced compartments from the Golgi apparatus and *trans*-Golgi network/early endosome are distinct in plant cells. *Plant J*. 2009:60(5):865–881. https://doi.org/10.1111/j.1365-313X.2009.04007.x

Li Y, Iqbal M, Zhang Q, Spelt C, Bliek M, Hakvoort HWJ, Quattrocchio FM, Koes R, Schat H. Two Silene vulgaris copper transporters residing in different cellular compartments confer copper hypertolerance by distinct mechanisms when expressed in *Arabidopsis thaliana*. *New Phytol*. 2017:215(3):1102–1114. https://doi.org/10.1111/nph.14647

Liu C, Li Z, Tian D, Xu M, Pan J, Wu H, Wang C, Otegui MS. AP1/2β-mediated exocytosis of tapetum-specific transporters is required for pollen development in *Arabidopsis thaliana*. *Plant Cell*. 2022:34(10):3961–3982. https://doi.org/10.1093/plcell/koac192

Liu D, Kumar R, Claus LAN, Johnson AJ, Siao W, Vanhoutte I, Wang P, Bender KW, Yperman K, Martins S, *et al*. Endocytosis of BRASSINOSTEROID INSENSITIVE1 is partly driven by a canonical tyr-based motif. *Plant Cell*. 2020:32(11):3598–3612. https://doi.org/10.1105/tpc.20.00384

Milner MJ, Seamon J, Craft E, Kochian LV. Transport properties of members of the ZIP family in plants and their role in Zn and Mn homeostasis. *J Exp Bot*. 2013:64(1):369–381. https://doi.org/10.1093/jxb/ers315

Obrdlik P, El-Bakkoury M, Hamacher T, Cappellaro C, Vilarino C, Fleischer C, Ellerbrok H, Kamuzinzi R, Ledent V, Blaudez D, *et al*. K+ channel interactions detected by a genetic system optimized for systematic studies of membrane protein interactions. *Proc Natl Acad Sci U S A*. 2004:101(33):12242–12247. https://doi.org/10.1073/pnas.0404467101

Park M, Song K, Reichardt I, Kim H, Mayer U, Stierhof YD, Hwang I, Jürgens G. Arabidopsis μ-adaptin subunit AP1 м of adaptor protein complex 1 mediates late secretory and vacuolar traffic and is required for growth. *Proc Natl Acad Sci U S A*. 2013:110(25):10318–10323. https://doi.org/10.1073/pnas.1300460110

Rehman M, Liu L, Wang Q, Saleem MH, Bashir S, Ullah S, Peng D. Copper environmental toxicology, recent advances, and future outlook: a review. *Environ Sci Pollut Res Int*. 2019:26(18):18003–18016. https://doi.org/10.1007/s11356-019-05073-6

Royle SJ. The cellular functions of clathrin. *Cell Mol Life Sci*. 2006:63(16):1823–1832. https://doi.org/10.1007/s00018-005-5587-0

Sancenón V, Puig S, Mira H, Thiele DJ, Peñarrubia L. Identification of a copper transporter family in *Arabidopsis thaliana*. *Plant Mol Biol*. 2003:51(4):577–587. https://doi.org/10.1023/A:1022345507112

Sanz A, Pike S, Khan MA, Carrió-Seguí À, Mendoza-Cózatl DG, Peñarrubia L, Gassmann W. Copper uptake mechanism of *Arabidopsis thaliana* high-affinity COPT transporters. *Protoplasma*. 2019:256(1):161–170. https://doi.org/10.1007/s00709-018-1286-1

Shabbir Z, Sardar A, Shabbir A, Abbas G, Shamshad S, Khalid S, Natasha, Murtaza G, Dumat C, Shahid M. Copper uptake, essentiality, toxicity, detoxification and risk assessment in soil-plant environment. *Chemosphere*. 2020:259:127436. https://doi.org/10.1016/j.chemosphere.2020.127436

Song W, Hu L, Ma Z, Yang L, Li J. Importance of tyrosine phosphorylation in hormone-regulated plant growth and development. *Int J Mol Sci*. 2022:23(12):6603. https://doi.org/10.3390/ijms23126603

Stenmark H. Rab GTPases as coordinators of vesicle traffic. *Nat Rev Mol Cell Biol*. 2009:10(8):513–525. https://doi.org/10.1038/nrm2728

Takano J, Tanaka M, Toyoda A, Miwa K, Kasai K, Fuji K, Onouchi H, Naito S, Fujiwara T. Polar localization and degradation of Arabidopsis boron transporters through distinct trafficking pathways. *Proc Natl Acad Sci U S A*. 2010:107(11):5220–5225. https://doi.org/10.1073/pnas.0910744107

Wang C, Hu T, Yan X, Meng T, Wang Y, Wang Q, Zhang X, Gu Y, Sánchez-Rodríguez C, Gadeyne A, *et al*. Differential regulation of clathrin and its adaptor proteins during membrane recruitment for endocytosis. *Plant Physiol*. 2016a:171(1):215–229. https://doi.org/10.1104/pp.15.01716

Wang C, Yan X, Chen Q, Jiang N, Fu W, Ma B, Liu J, Li C, Bednarek SY, Pan J. Clathrin light chains regulate clathrin-mediated trafficking, auxin signaling, and development in Arabidopsis. *Plant Cell*. 2013b:25(2):499–516. https://doi.org/10.1105/tpc.112.108373

Wang JG, Feng C, Liu HH, Ge FR, Li S, Li HJ, Zhang Y. HAPLESS13-mediated trafficking of STRUBBELIG is critical for ovule development in Arabidopsis. *PLOS Genet*. 2016b:12(8):e1006269. https://doi.org/10.1371/journal.pgen.1006269

Wang JG, Li S, Zhao XY, Zhou LZ, Huang GQ, Feng C, Zhang Y. HAPLESS13, the Arabidopsis μ1 adaptin, is essential for protein sorting at the *trans*-Golgi network/early endosome. *Plant Physiol*. 2013a:162(4):1897–1910. https://doi.org/10.1104/pp.113.221051

Wang S, Yoshinari A, Shimada T, Hara-Nishimura I, Mitani-Ueno N, Ma JF, Naito S, Takano J. Polar localization of the NIP5;1 boric acid

channel is maintained by endocytosis and facilitates boron transport in Arabidopsis roots. *Plant Cell*. 2017:29(4):824–842. https://doi.org/10.1105/tpc.16.00825

Xu E, Liu Y, Gu D, Zhan X, Li J, Zhou K, Zhang P, Zou Y. Molecular mechanisms of plant responses to copper: from deficiency to excess. *Int J Mol Sci*. 2024:25(13):6993. https://doi.org/10.3390/ijms25136993

Xu M, Yan X, Wang Y, Liu C, Yang Q, Tian D, Bednarek SY, Pan J, Wang C. ADAPTOR PROTEIN-1 complex-mediated post-Golgi trafficking is critical for pollen wall development in Arabidopsis. *New Phytol*. 2022:235(2):472–487. https://doi.org/10.1111/nph.18170

Yamaoka S, Shimono Y, Shirakawa M, Fukao Y, Kawase T, Hatsugai N, Tamura K, Shimada T, Hara-Nishimura I. Identification and dynamics of Arabidopsis adaptor protein-2 complex and its involvement in floral organ development. *Plant Cell*. 2013:25(8): 2958–2969. https://doi.org/10.1105/tpc.113.114082

Yan X, Wang Y, Xu M, Dahhan DA, Liu C, Zhang Y, Lin J, Bednarek SY, Pan J. Cross-talk between clathrin-dependent post-Golgi trafficking and clathrin-mediated endocytosis in Arabidopsis root cells. *Plant Cell*. 2021:33(9):3057–3075. https://doi.org/10.1093/plcell/koab180

Yao HY, Xue HW. Signals and mechanisms affecting vesicular trafficking during root growth. *Curr Opin Plant Biol*. 2011:14(5): 571–579. https://doi.org/10.1016/j.pbi.2011.06.009

Yao S, Kang J, Guo G, Yang Z, Huang Y, Lan Y, Zhou T, Wang L, Wei C, Xu Z, *et al*. The key micronutrient copper orchestrates broad-

spectrum virus resistance in rice. *Sci Adv*. 2022:8(26):eabm0660. https://doi.org/10.1126/sciadv.abm0660

Yoshinari A, Fujimoto M, Ueda T, Inada N, Naito S, Takano J. DRP1-dependent endocytosis is essential for polar localization and boron-induced degradation of the borate transporter BOR1 in *Arabidopsis thaliana*. *Plant Cell Physiol*. 2016:57(9):1985–2000. https://doi.org/10.1093/pcp/pcw121

Yoshinari A, Hosokawa T, Amano T, Beier MP, Kunieda T, Shimada T, Hara-Nishimura I, Naito S, Takano J. Polar localization of the borate exporter BOR1 requires AP2-dependent endocytosis. *Plant Physiol*. 2019:179(4):1569–1580. https://doi.org/10.1104/pp.18.01017

Zhang WJ, Zhou Y, Zhang Y, Su YH, Xu T. Protein phosphorylation: a molecular switch in plant signaling. *Cell Rep*. 2023:42(7):112729. https://doi.org/10.1016/j.celrep.2023.112729

Zhang Y, Yu Q, Jiang N, Yan X, Wang C, Wang Q, Liu J, Zhu M, Bednarek SY, Xu J, *et al*. Clathrin regulates blue light-triggered lateral auxin distribution and hypocotyl phototropism in Arabidopsis. *Plant Cell Environ*. 2017:40(1):165–176. https://doi.org/10.1111/pce.12854

Zhang Z, Fu D, Sun Z, Ju C, Miao C, Wang Z, Xie D, Ma L, Gong Z, Wang C. Tonoplast-associated calcium signaling regulates manganese homeostasis in Arabidopsis. *Mol Plant*. 2021:14(5):805–819. https://doi.org/10.1016/j.molp.2021.03.003